J. Fluid Mech. (1990), *vol.* 212, *pp.* 451–485
Printed in Great Britain

On transition to chaos in two-dimensional channel flow symmetrically driven by accelerating walls

By E. B. B. WATSON, W. H. H. BANKS, M. B. ZATURSKA AND P. G. DRAZIN

School of Mathematics, University Walk, Bristol BS8 1TW, UK

(Received 31 October 1988)

We study theoretically the flow of a viscous incompressible fluid in a parallel-walled channel: the flow is driven by uniform steady suction through the porous and accelerating walls of the channel. Previous authors have discussed special cases of such flows, confining attention to flows which are symmetric, steady and two-dimensional; a similarity form of solution is assumed, as used by Berman and originally due to Hiemenz, to reduce the Navier–Stokes equations to a nonlinear ordinary differential equation. We generalize their work by considering asymmetric flows, unsteady flows and three-dimensional perturbations. By use of numerical calculations, matched asymptotic expansions for large values of the Reynolds number, both positive and negative, and the theory of dynamical systems we find many more exact solutions of the Navier–Stokes equations, examine their stability and interpret them; although much of the theory is for the general case, most of the numerical calculations are for the case of zero suction. In particular we show that most of the previously found steady solutions are unstable to antisymmetric two-dimensional disturbances. This leads to a pitchfork bifurcation, stable asymmetric steady solutions, a Hopf bifurcation, stable time-periodic solutions, stable quasi-periodic solutions and chaos in succession as the Reynolds number increases from zero, and a pitchfork bifurcation, stable asymmetric steady solutions, a Hopf bifurcation, periodic solutions, chaos via period doubling, other periodic solutions and chaos in succession as the Reynolds number decreases from zero.

1. Introduction

The so-called exact solutions of the Navier–Stokes equations have been of practical importance and theoretical interest for a long time. Such solutions range from simple and analytic to complicated three-dimensional and numerical ones. Well-known examples are Poiseuille flow in a pipe, two-dimensional stagnation-point flow and uniform flow past a sphere. The essential difference of the last of these is that the solution depends on a parameter, namely the Reynolds number; also, as in the second example, the solution is found by numerical means. In the present paper we shall examine other exact solutions of the Navier–Stokes equations, which describe two-dimensional flows in a channel.

The steady laminar flow of an incompressible viscous fluid along a channel with rigid porous walls has already received much attention. Berman (1953) assumed a similarity form of solution and reduced the problem to a single nonlinear fourth-order ordinary differential equation with two boundary conditions at each wall. This exact solution of the Navier–Stokes equations has been generalized and extended by, e.g., Terrill (1964), Durlofsky & Brady (1984) and Zaturska, Drazin & Banks (1988,

henceforth referred to as ZDB). The similarity form has a long history – it was originally applied by Hiemenz to flow at a stagnation point, and has most recently been applied by Stuart (1988) to the development of a singularity in the flow of an inviscid fluid at a finite time.

In the present paper we formulate a closely related problem, the flow of a viscous incompressible fluid driven along a channel with porous uniformly accelerating rigid walls. We shall use the same similarity form of solution as Berman: the resulting differential equation is identical to that for porous-channel flow, only the boundary conditions differ. The flow with zero suction was previously examined by Brady & Acrivos (1981), who also made use of the same similarity form. Moreover they described the importance and physical context of the problem, and found many interesting results. Here we find new solutions, periodic in time as well as steady, and examine the stability of these exact solutions, finding a rich structure of multiple equilibria. Our investigation, although concerned principally with the case of zero suction, closely parallels the work of ZDB, so we shall state the problem without more ado.

The problem is modelled as follows. The channel walls have equations $y = \pm h$ and the velocity components of a two-dimensional flow are u, v in $-\infty < x < \infty$, $-h < y < h$. The stream function ψ satisfies the vorticity equation

$$\frac{\partial \nabla^2 \psi}{\partial t} + \frac{\partial(\nabla^2 \psi, \psi)}{\partial(x, y)} = \nu \nabla^4 \psi, \tag{1.1}$$

where $u = \partial\psi/\partial y$, $v = -\partial\psi/\partial x$, t represents the time and ν is the kinematic viscosity of the fluid. The boundary conditions corresponding to porous accelerating walls are

$$u = Ex, \quad v = \pm V \quad \text{at} \quad y = \pm h. \tag{1.2}$$

We henceforth non-dimensionalize length with respect to h, and time with respect to $(E + V/h)^{-1}$, introducing the Reynolds number defined by $R = (V + Eh)\, h/\nu$. We shall see soon that when $V + Eh = 0$ the problem becomes a limiting case of a more general formulation.

Similarity solutions of Berman's form

$$\psi(x, y, t, R) = xf(y, t, R) \tag{1.3}$$

are sought, for which the corresponding velocity components are

$$u = xf_y, \quad v = -f. \tag{1.4}$$

The vorticity equation becomes

$$f_{yyt} = R^{-1} f_{yyyy} + f f_{yyy} - f_y f_{yy} \tag{1.5}$$

with boundary conditions

$$f = \mp(1 - \chi), \quad f_y = \chi \quad \text{at} \quad y = \pm 1, \tag{1.6}$$

where $\chi = Eh/(V + Eh)$. An initial condition is required to pose the problem for $f(y, t, R)$, but we delay consideration of it until §7. Steady solutions correspond to

$$\psi(x, y, R) = xF(y, R), \tag{1.7}$$

so that F satisfies

$$F^{\mathrm{iv}} + R(FF''' - F'F'') = 0, \tag{1.8}$$

$$\mathbf{B}F = [1 - \chi,\ \chi,\ -1 + \chi,\ \chi]^{\mathrm{T}}, \tag{1.9}$$

where the vector operator $\mathbf{B}$ is defined by $\mathbf{B}F = [F(-1), F'(-1), F(1), F'(1)]^{\mathrm{T}}$ and a

prime denotes differentiation with respect to y. The parameter χ may take any real value, and the case $\chi = 0$ represents steady flow in a porous channel (see ZDB for history and details) and that of $\chi = 1$ the accelerating-wall flow investigated by Brady & Acrivos (1981). The special case $V+Eh = 0$ corresponds to χ infinite and represents either suction with the wall moving towards the origin or injection with the wall moving away from the origin. We shall collect the results for this case in the Appendix. It is opportune also now to introduce the operators $\mathbf{B}_S$ and $\mathbf{B}_A$ such that

$$\mathbf{B}_S F = [F(-1), F'(-1), F(0), F''(0)]^T \tag{1.10}$$

and

$$\mathbf{B}_A F = [F(-1), F'(-1), F'(0), F'''(0)]^T. \tag{1.11}$$

It is often more convenient to use the integral of (1.8),

$$F''' + R(FF'' - F'^2) + \beta = 0, \tag{1.12}$$

where $\beta = R\{\chi^2 + (1-\chi)F''(1)\} - F'''(1)$ is the constant of integration.

The basic flow governed by (1.8) subject to symmetric boundary conditions $\mathbf{B}_S F = [0, 1, 0, 0]^T$ with $\chi = 1$ has been studied by Brady & Acrivos (1981). We first summarize their results. For $0 < R < R_3$ there is a single solution, while for $R > R_3$ there are three solutions, where $R_3 \approx 310$. The multiple solutions correspond to distinct values of the integration constant β but all have the same skin friction $F''(1, R)$ for given large R. The single solution is said to be of type I, the other two of types II and III. Durlofsky & Brady (1984) found, but did not present directly, solutions of type I for $R < 0$, their principal concern being with spatial growth of disturbances. In our study we have concentrated on solutions of type I and their bifurcations because we anticipate that the flows of types II and III are unstable (cf. ZDB): the symmetric solutions of type I are the only set of solutions that exists for all values of R. A plot of the state variable $F''(1, R)$ versus R for solutions of type I is presented in figure 1.

In order to examine the temporal stability of such steady flows for general χ we write

$$f(y, t, R) = F(y, R) + g(y, t, R), \tag{1.13}$$

linearize (1.5) for small g and seek normal modes with

$$g(y, t, R) = e^{st} G(y, R). \tag{1.14}$$

Then an eigenfunction G satisfies

$$G^{iv} + R(FG''' - F'G'' - F''G' + F'''G) = RsG'', \tag{1.15}$$

$$\mathbf{B}G = \mathbf{0}, \tag{1.16}$$

for eigenvalue s. A specified basic flow with $V+Eh > 0$ is unstable if $\mathrm{Re}\,(s) > 0$ for at least one eigenvalue, and one with $V+Eh < 0$ is unstable if $\mathrm{Re}\,(s) < 0$ for at least one eigenvalue (because, with the timescale $(E+V/h)^{-1}$ we have chosen, time is apparently reversed when $V+Eh < 0$). The case $V+Eh = 0$ is discussed in the Appendix. For a symmetric flow, F is an odd function of y and so each eigenfunction G is either an even function (i.e. an antisymmetric mode) or an odd function of y (i.e. a symmetric mode); then in effect we may solve (1.15) with either boundary conditions $\mathbf{B}_A G = \mathbf{0}$ or $\mathbf{B}_S G = \mathbf{0}$ respectively, for which we denote the eigenvalue by $s = q_n$ or $s = r_n$ respectively for $n = 1, 2, \ldots$.

The spatial stability of the steady solutions for $\chi = 0$ and 1 has been examined by Durlofsky & Brady (1984), who essentially expressed

$$\psi(x, y, R) = xF(y, R) + h(x, y, R), \tag{1.17}$$

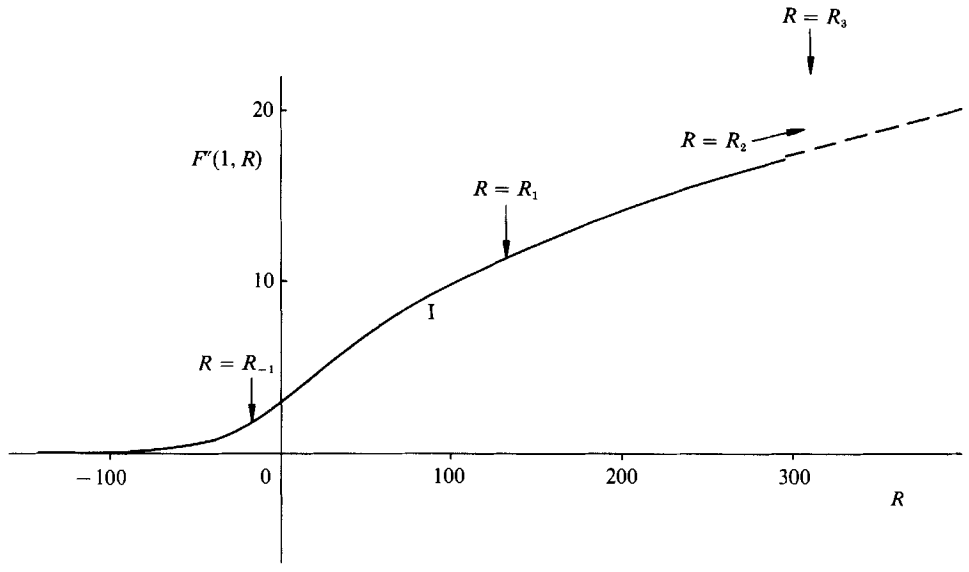

FIGURE 1. Values of $F''(1,R)$ $(= -F''(-1,R))$ versus R for the symmetric solutions of type I with $\chi = 1$. We have labelled some critical values which we describe later. The dashed curve represents the asymptotic result (2.16).

linearized (1.8) for small h, considered spatial modes of the form

$$h(x,y,R) = x^{\lambda}H(y,R) \tag{1.18}$$

and neglected small terms as $x \to \infty$. This gives rise to the problem

$$H^{\mathrm{iv}} + R(FH''' - F''H') = \lambda R(F'H'' - F'''H), \tag{1.19}$$

$$\mathbf{B}H = \mathbf{0}, \tag{1.20}$$

for eigenfunctions H with eigenvalues λ. Durlofsky & Brady considered only symmetric modes; they found that when $\chi = 1$ there are only negative eigenvalues for $R < 0$, only positive eigenvalues for $0 < R < 11.0$ and both positive and negative eigenvalues for $R > 11.0$. All their negative eigenvalues satisfy $\lambda < -2$, all the positive ones $\lambda > 1$. It is noteworthy that the spatial eigenvalue problem (1.19), (1.20) coincides with the temporal eigenvalue problem (1.15), (1.16) when there is neutral stability, i.e. when $\lambda = 1$ and $s = 0$.

We shall describe some asymptotic properties of the steady flows, as defined by (1.8) and (1.9), and their eigenvalues as $R \to 0$ and $R \to \pm\infty$ in §2. In §3 we present for the case $\chi = 1$ numerical results about the steady solutions and their instabilities. In particular we find that the well-known steady solutions in which $F'(y)$ is symmetric about the centreline of the channel become unstable and bifurcate into pairs of asymmetric solutions at two critical values of the Reynolds number, one positive and one negative; these asymmetric solutions in turn become unstable as $|R|$ increases further. Section 4 comprises a local analysis of the bifurcations of all steady solutions for arbitrary χ. In §5 we discuss for the case $\chi = 1$ asymptotic properties of the asymmetric solutions and of the eigenvalue problems associated with them. Some properties of three-dimensional instability of the steady two-dimensional solutions are presented in §6. In §7 the results of direct numerical integration of the partial differential system (1.5), (1.6) with $\chi = 1$ are described: these confirm many of our previous results and show many bifurcations along the route to chaos.

It may help the reader of this long and technical paper to describe its spirit in one paragraph. Although the experimental realization of the theoretical model with *two* accelerating walls does not seem feasible, that in which only the bottom wall of the channel is accelerating might, with difficulty, be achieved by moving a very dense liquid, such as mercury, over a suitably shaped bed. In any case, the model is relevant to other flows such as flow near a stagnation point and flow of a light fluid near a dense one. Also the model more importantly describes a special class of exact solutions of the Navier–Stokes equations which offers a paradigm for many aspects of transition to turbulence. Indeed the problem is of didactic value for its encapsulation of the theory of hydrodynamic instability of flow with symmetry and consequent symmetry breaking. The symmetry group of the problem corresponds to the symmetry of the channel in its centreline. The dynamics of the transition and chaos described in §7 is crucially influenced by the existence of the unstable steady and time-periodic flows elucidated at length in §§2–5. However, if the reader is impatient to learn about the appearance of chaos then he or she may proceed at once to §7.

The problem has many solutions with an interesting structure and many kinds of bifurcation arise; as a result it was found necessary to use what may appear to be a complicated notation for the values of R at the bifurcation points. In view of this, the notation is summarized here. We first recall that the steady symmetric flows are classified as being of types I, II or III. The values of R where steady asymmetric flows first bifurcate from steady symmetric flows of type I as $|R|$ increases are denoted by R_{-1}, R_1 (pitchforks): a subscript minus denotes, here and henceforth, that the value of R is negative. Continuing along the type I branch with $R > 0$ we use R_2, R_3 for the turning points distinguishing type II and type III flows; the values of R at Hopf bifurcations, where time-periodic flows bifurcate from steady asymmetric flows, are denoted by R_{-11} and R_{11}; the (negative) values of R where the periods of flows double are denoted by $R^{(1)}, R^{(2)}, \ldots$. Finally, we denote by I_{-1}, I_1 the types of asymmetric steady flows bifurcating at R_{-1}, R_1 respectively, and in addition denote by I'_{-1}, I'_1 the 'reflected' flows in the centreline of the channel, corresponding to the symmetry of the problem.

2. Asymptotic results for small and large R

In §3 we shall describe the numerical integration of the equations for the basic steady flow F and the eigensolutions G, s of its temporal modes, but it is convenient first to use some asymptotic methods. By so doing we find results about the basic flow and its eigensolutions not only to compare with the numerical results but also to be continued numerically as $|R|$ increases from zero and to join the numerical results as $|R|$ decreases from infinity.

2.1. *Analysis for small R*

Assuming the expansion

$$F(y,R) = F_0(y) + RF_1(y) + \ldots \quad \text{as} \quad R \to 0, \tag{2.1}$$

substituting it into the problem (1.8), (1.9) for steady flows, and equating sucessive powers of R, we find at length (following Terrill 1964 and Brady 1981) that

$$F_0(y) = \tfrac{1}{2}y(y^2-3) + \chi y, \quad F_1(y) = \tfrac{1}{280}y(y^6-3y^2+2), \ldots. \tag{2.2}$$

For each value of χ this gives the unique steady solution, namely the symmetric solution of type I, for small values of R.

At the same time we may also expand the eigensolution (Watson 1987 and ZDB) in the form

$$G(y,R) = G_0(y)+RG_1(y)+\ldots, \quad s(R) = R^{-1}s_{-1}+s_0+Rs_1+\ldots \quad \text{as} \quad R\to 0, \quad (2.3)$$

substitute expansions (2.1) and (2.3) into the eigenvalue problem (1.15), (1.16) and equate successive powers of R. This at length gives the antisymmetric modes (with $s = q_n$), where

$$q_n(R) = -n^2\pi^2/R - 21/8n^2\pi^2 + \tfrac{5}{2}(1-\chi) + O(R),$$

and

$$G(y,R) = \cos n\pi y - (-1)^n + O(R) \quad \text{as} \quad R\to 0; \quad (2.4)$$

and similarly it gives the symmetric modes (with $s = r_n$), where

$$r_n(R) = -\mu_n^2/R + 55/8\mu_n^2 + \tfrac{5}{2}(1-\chi) + O(R),$$

$$G(y,R) = y - \sin(\mu_n y)/\sin\mu_n + O(R) \quad \text{as} \quad R\to 0, \quad (2.5)$$

and μ_n is defined as the nth positive root of $\tan\mu = \mu$ (which is tabulated by Abramowitz & Stegun (1964, p. 224)).

Brady (1981) and Watson (1987) give many further details for the case $\chi = 1$, and ZDB for the case $\chi = 0$, showing how well these asymptotic results agree with direct numerical calculations.

2.2. *Analysis for large positive R*

The assumed structure of the asymptotic solutions below is based on the literature (especially Terrill 1964 and Brady & Acrivos 1981), numerical results, and trial and error. For brevity we shall merely summarize the results without detailed justification, the essential justification being that the assumptions lead to a self-consistent asymptotic solution and that a comparison of numerical and asymptotic results gives confidence in the validity of the structure of the solution. We have the two sub-cases $\chi = 1$ and $\chi \neq 1$.

2.2.1. $\chi = 1$

When $\chi = 1$ the steady symmetric flows of type I have a boundary layer of thickness of order of magnitude $R^{-\frac{1}{2}}$ near each wall and are essentially inviscid elsewhere when R is large. In mathematical terms we assume that there is an outer solution of the form $F(y,R) = R^{-\frac{1}{2}}\Phi(y,R)$, where

$$\Phi(y,R) = \Phi_0(y)+R^{-\frac{1}{2}}\Phi_1(y)+\ldots \quad \text{as} \quad R\to\infty \quad \text{for fixed} \quad y \neq \pm 1 \quad (2.6)$$

and Φ satisfies the outer boundary conditions that

$$\Phi(-1) = 0 \quad \text{to leading order and} \quad \Phi(0) = \Phi''(0) = 0. \quad (2.7)$$

We also assume that there is an inner solution of the form $F(y,R) = R^{-\frac{1}{2}}\phi^+(\eta,R)$, where

$$\eta = R^{\frac{1}{2}}(1+y), \quad (2.8)$$

$$\phi^+(\eta,R) = \phi_0^+(\eta)+R^{-\frac{1}{2}}\phi_1^+(\eta)+\ldots \quad \text{as} \quad R\to\infty \quad \text{for fixed} \quad \eta, \quad (2.9)$$

and ϕ^+ satisfies the inner boundary conditions that

$$\phi^+(0) = 0, \quad \phi^{+\prime}(0) = 1. \quad (2.10)$$

There will, of course, be a similar boundary layer near $y = 1$. Finally, we assume that the inner and outer solutions match at the edge of the boundary layer, i.e. that

$$\lim_{y\downarrow 0}\Phi(y,R) \sim \lim_{\eta\uparrow\infty}\phi^+(\eta,R) \quad \text{as} \quad R\to\infty. \quad (2.11)$$

With these assumptions (1.8) or (1.12) may be solved at successive orders of approximation. We find at length that

$$\Phi_0(y) = -y, \tag{2.12}$$

$$\phi_0^+(\eta) = 1-\mathrm{e}^{-\eta}, \tag{2.13}$$

$$\Phi_1(y) = -(1+\mathrm{I})\,y \tag{2.14}$$

and

$$\phi_1^+(\eta) = -\tfrac{1}{4}\mathrm{e}^{-(\eta+1)}\int_0^\eta (1+\mathrm{e}^v)\left\{\int_0^v \exp\left(\int_0^u \frac{3+\mathrm{e}^{-x}}{1+\mathrm{e}^x}\,\mathrm{d}x\right)\mathrm{d}u\right\}\mathrm{d}v, \tag{2.15}$$

where

$$\mathrm{I} = \int_0^1 [\mathrm{e}^{-s}\{(1+s)^{-1}+(1+s)^{-2}-s^{-1}\}+s^{-1}]\,\mathrm{d}s = 1.6126.$$

Watson (1987) gives further details of the asymptotic analysis and its successful comparison with direct numerical integration of the problem (1.8), (1.9). In particular, the result

$$F''(1) = R^{\frac{1}{2}}+1/2\mathrm{e}+O(R^{-\frac{1}{2}}) \quad \text{as} \quad R\to\infty \tag{2.16}$$

gives the asymptote to the curve for the solution of type I in figure 1.

Brady & Acrivos (1981, §2.4) discuss some asymptotic results as $R\to\infty$ for the solutions of types II and III.

We may use the asymptotic solution obtained above to investigate the eigenvalues corresponding to type I solutions for large positive R. Replacing F by $-\alpha y$, where $\alpha = R^{-\frac{1}{2}}+2.6126R^{-1}+\ldots$, we approximate (1.15) for the eigenfunctions by

$$\Gamma^{\mathrm{iv}}-R\alpha y\Gamma''-R(s-\alpha)\,\Gamma'' = 0, \tag{2.17}$$

where $\Gamma(y,R)$ denotes the inviscid representation of $G(y,R)$. The boundary conditions at $y=0$ are $\Gamma=\Gamma''=0$ for the symmetric, and $\Gamma=\Gamma''=0$ for the antisymmetric, modes. The general solution of (2.17) is

$$\Gamma''(y,R) = \exp(\tfrac{1}{4}\alpha R y^2)\left\{AU\left(\frac{s}{\alpha}-\tfrac{3}{2},(\alpha R)^{\frac{1}{2}}y\right)+BV\left(\frac{s}{\alpha}-\tfrac{3}{2},(\alpha R)^{\frac{1}{2}}y\right)\right\}, \tag{2.18}$$

where A, B are constants and U, V are the parabolic cylinder functions. We assume here that the normalization (e.g. $G''(-1)=1$ in our numerical work) of the eigenfunctions is of order of magnitude one and that therefore the eigenfunctions are not exponentially large in R. The asymptotic behaviour of U, V, corresponding to large R, is given in Abramowitz & Stegun (1964) and we note that Γ'' is exponentially large for $y\neq 0$ unless B is exponentially small. It follows that

$$\Gamma''(0,R) = A\pi^{\frac{1}{2}}\{2^{(s/\alpha-1)/2}(s/2\alpha-1)!\}$$

to leading order, and so for the symmetric modes we obtain the eigenvalues

$$r_n \sim 2\alpha(1-n) \quad \text{as} \quad R\to\infty \quad (n=1,2,\ldots). \tag{2.19}$$

Similarly, the eigenvalues for the antisymmetric modes are obtained from the condition that $U'(s/\alpha-\frac{3}{2},0)=0$ and we find

$$q_n \sim \alpha(3-2n) \quad \text{as} \quad R\to\infty \quad (n=1,2,\ldots). \tag{2.20}$$

We note here that, as for $|R|\ll 1$, the symmetric and antisymmetric eigenvalues interlace but they all tend to zero as $R\to\infty$. However, $q_1\downarrow 0$ as $R\to\infty$ and since $q_1<0$ for $R\ll 1$ we may infer the existence of a zero of q_1 at finite R.

2.2.2. $\chi \neq 1$

For this case the steady symmetric flows of type I are found to have a boundary layer of thickness R^{-1} near each wall and are inviscid elsewhere when R is large. We therefore assume an outer solution of the form $F(y,R) = \Phi(y,R)$, where

$$\Phi(y,R) = \Phi_0(y) + R^{-1}\Phi_1(y) + \ldots \quad \text{as} \quad R \to \infty \quad \text{for fixed} \quad y \neq \pm 1 \tag{2.21}$$

and Φ satisfies the outer boundary conditions, namely

$$\Phi(-1) = 1-\chi \quad \text{to leading order and} \quad \Phi(0) = \Phi''(0) = 0. \tag{2.22}$$

Further, we assume that there is an inner solution of the form $F(y,R) = \phi^+(\eta,R)$, where

$$\eta = R(1+y), \tag{2.23}$$

$$\phi^+(\eta,R) = \phi_0^+(\eta) + R^{-1}\phi_1^+(\eta) + \ldots \quad \text{as} \quad R \to \infty \quad \text{for fixed} \quad \eta, \tag{2.24}$$

and ϕ^+ satisfies the inner boundary conditions

$$\phi^+(0) = 1-\chi, \quad \phi^{+\prime}(0) = \chi. \tag{2.25}$$

The inner and outer solutions are matched at the edge of the boundary layer by condition (2.11). (It was found from the matching that additional terms in $R^{-\frac{1}{2}}$ in the inner and outer solutions are inadmissible.)

Solving (1.8) at successive orders of approximation we find that

$$\Phi_0(y) = -(1-\chi)\,y, \tag{2.26}$$

$$\phi_0^+(\eta) = 1-\chi, \tag{2.27}$$

$$\Phi_1(y) = -(1-\chi)^{-1}y \tag{2.28}$$

and

$$\phi_1^+(\eta) = -(1-\chi)^{-1}\mathrm{e}^{-(1-\chi)\eta} - (1-\chi)\eta + (1-\chi)^{-1}. \tag{2.29}$$

It is apparent from (2.28) and (2.29) why a different scaled variable is required for the case $\chi = 1$.

From the results (2.26)–(2.29) we obtain

$$F''(-1) = -R(1-\chi) + (1-2\chi)\,(1-\chi)^{-1} + o(1) \tag{2.30}$$

and

$$F'(0) = -(1-\chi) - R^{-1}(1-\chi)^{-1} + o(R^{-1}) \quad \text{as} \quad R \to \infty. \tag{2.31}$$

There is good agreement between the numerical and analytical results: for example, when $\chi = \frac{1}{2}$ and $R = 100$, the 'exact' numerical results are $F''(-1) = -49.64308$ and $F'(0) = -0.52407$, whereas from (2.30) and (2.31) we obtain values of -50.0 and -0.52 respectively.

The analysis for the eigenvalues corresponding to this flow as $R \to \infty$ follows that for $\chi = 1$. Results (2.19), (2.10) still apply but with α given by $\alpha = (1-\chi) + (1-\chi)^{-1}R^{-1} + \ldots$. Note that, as for $\chi = 1$, q_1 has a zero for $\chi \neq 1$. Apart from the cases $\chi = 0$ (ZDB) and $\chi = 1$ (this study) we have not obtained numerical results for comparison.

We also note that an analysis similar to the above, but applied to the spatial eigenvalue problem (1.19), (1.20), leads to the antisymmetric and symmetric eigenvalues

$$l_n \to 2(n-1), \quad m_n \to 2n-1 \quad \text{for} \quad n = 1, 2, \ldots \quad \text{as} \quad R \to \infty$$

respectively. Note that these results are independent of χ, but for $\chi = 0$ and 1 Durlofsky & Brady (1984) state, on the evidence of their numerical results, that $m_1 \to 1$ as $R \to \infty$. As in the analysis of temporal stability, we note that since $l_1 \to 0$ as

$R \to \infty$ and $l_1 > 1$ as $R \to 0$, it follows that $l_1 - 1$ vanishes for some finite value of R, at which there is neutral stability. Indeed, as indicated earlier, if there is temporal neutral stability at a particular value of R, then there is spatial neutral stability at that value of R.

2.3. *Analysis for large negative R*

The structure of the asymptotic solution is here based on the work of Terrill (1965). The unique steady symmetric flow of type I has a shear layer, with thickness of order of magnitude $(-R)^{-\frac{1}{2}}$, near the centre of the channel and is inviscid elsewhere as $R \to -\infty$. There is no fundamental distinction in this case between $\chi = 1$ and $\chi \neq 1$. It is convenient first to write $F(y,R) = \mathscr{F}(\theta,\epsilon)$ where $\theta = \zeta y$, $\epsilon = -\zeta/R$ and the positive parameter ζ will be defined later in terms of χ. We next assume an outer solution of the form $\mathscr{F}(\theta,\epsilon) = \Phi(\theta,\epsilon)$, where

$$\Phi(\theta,\epsilon) = \Phi_0(\theta) + \epsilon\Phi_1(\theta) + \ldots \quad \text{as} \quad \epsilon \to 0 \quad \text{for fixed} \quad \theta \neq 0 \tag{2.32}$$

and Φ satisfies the outer boundary conditions

$$\Phi(1) = -(1-\chi), \quad \Phi'(1) = \chi \quad \text{and} \quad \Phi(0) = 0 \quad \text{to leading order.} \tag{2.33}$$

We also assume an inner solution of the form $\mathscr{F}(\theta,\epsilon) = \epsilon^{\frac{1}{2}}\phi^-(\xi,\epsilon)$ where

$$\xi = \theta\epsilon^{-\frac{1}{2}}, \tag{2.34}$$

$$\phi^-(\xi,\epsilon) = \phi_0^-(\xi) + \epsilon\phi_1^-(\xi) + \epsilon^2 \ln\epsilon\,\phi_2^-(\xi) + \epsilon^2\phi_3^-(\xi) + \ldots \quad \text{as} \quad \epsilon \to 0 \quad \text{for fixed} \quad \xi \tag{2.35}$$

and ϕ^- satisfies the inner boundary conditions,

$$\phi^-(0) = \phi^{-\prime\prime}(0) = 0. \tag{2.36}$$

Finally we assume that the solutions match at the edge of the shear layer, i.e.

$$\lim_{\theta\to 0} \Phi(\theta,\epsilon) \sim \lim_{\xi\to\infty} \epsilon^{\frac{1}{2}}\phi^-(\xi,\epsilon) \quad \text{as} \quad \epsilon \to 0.$$

Solving at successive orders of approximation, we find that

$$\Phi_0(\theta) = A_0 \sin\theta, \tag{2.37}$$

where $$A_0 = -\{(1-\chi)^2 + \chi^2\zeta^{-2}\}^{\frac{1}{2}}$$

and ζ is the first positive root of $\tan\zeta = -(\chi^{-1}-1)\zeta$. We note that $\zeta = \frac{1}{2}\pi$ and $A_0 = -1$ for pure injection ($\chi = 0$), while $\zeta = \pi$ and $A_0 = -\pi^{-1}$ for the accelerating-wall flow ($\chi = 1$). Further,

$$\phi_0^-(\xi) = A_0\xi, \tag{2.38}$$

$$\Phi_1(\theta) = B_1(\sin\theta - \theta\cos\theta) + \frac{\gamma_1}{2A_0}\sin\theta - \tfrac{1}{2}(\theta\cos\theta - \sin\theta)\ln(\tan\tfrac{1}{2}\theta) + \tfrac{1}{2}\cos\theta\int_0^\theta \frac{\theta\,\mathrm{d}\theta}{\sin\theta} \tag{2.39}$$

and

$$\phi_1^-(\xi) = -\tfrac{1}{6}A_0\xi^3 + \left(\frac{\gamma_1}{2A_0} + \tfrac{1}{2}\right)\xi, \tag{2.40}$$

where

$$B_1 = -\frac{\dfrac{\gamma_1}{2A_0}\sin\zeta - \tfrac{1}{2}(\zeta\cos\zeta - \sin\zeta)\ln(\tan\tfrac{1}{2}\zeta) + \tfrac{1}{2}\cos\zeta\displaystyle\int_0^\zeta \frac{\theta\,\mathrm{d}\theta}{\sin\theta}}{\sin\zeta - \zeta\cos\zeta}$$

and

$$\frac{\gamma_1}{A_0} = \frac{\{\sin\zeta + (1-\chi)\,\zeta\cos\zeta\}\displaystyle\int_0^\zeta \frac{\theta\,\mathrm{d}\theta}{\sin\theta} - 1}{\cos\zeta - (1-\chi)\sin\zeta}.$$

With $\chi = 0$, we find

$$A_0 = -1, \quad \gamma_1 = \frac{2}{\pi}\left(\int_0^{\frac{1}{2}\pi} \frac{\theta \, d\theta}{\sin\theta} - 1\right), \quad B_1 = \tfrac{1}{2}\gamma_1,$$

in agreement with Terrill (1965), while with $\chi = 1$, we find $A_0 = \gamma_1 = -\pi^{-1}$ and $B_1 = 0$. Consequences of these latter values are

$$F'(0,R) = -1 - \pi^2 R^{-1} + o(R^{-1}), \quad F''(1,R) = o(R^{-1}),$$

$$F(\tfrac{1}{2},R) = -\pi^{-1} - \tfrac{1}{2}\pi R^{-1} + o(R^{-1}), \quad F'(\tfrac{1}{2},R) = -\pi^2\left(1 - \int_0^{\frac{1}{2}\pi} \frac{\theta \, d\theta}{\sin\theta}\right)/2R + o(R^{-1})$$

and

$$F''(\tfrac{1}{2},R) = \pi + \tfrac{1}{2}\pi^3 R^{-1} + o(R^{-1}) \quad \text{as} \quad R \to -\infty.$$

For $R = -2000$ exact numerical solutions compared with these five asymptotic results are -1.00494 versus -1.00493, 0.00140 versus 0, -0.31751 versus -0.31752, -0.00204 versus -0.00205 and 3.13364 versus 3.13384 respectively. When $\chi = \frac{1}{2}$ we find $F'(0,R) = -1.13094 - 1.74968R^{-1} + o(R^{-1})$, $F''(1,R) = 2.05793 - 5.51035R^{-1} + o(R^{-1})$ with corresponding exact and asymptotic values at $R = -200$ of -1.12274 versus -1.12219 and 2.08562 versus 2.08548 respectively.

We may use the asymptotic solutions obtained above to investigate the eigenvalues corresponding to type I solutions for large negative R. For general values of χ we were able, by substituting the outer solution for F into (1.15), to find one eigenfunction $G(y,R) = \cos\theta - \cos\zeta$ with corresponding eigenvalue $-\chi$; from the special case $\chi = 1$, a discussion of which follows, we may identify this eigenvalue as q_1.

When $\chi = 1$ we assume an outer representation $G(y,R) = \Gamma(\theta,\epsilon)$ for the eigenfunction, where

$$\Gamma(\theta,\epsilon) = \Gamma_0(\theta) + \epsilon\Gamma_1(\theta) + \ldots \quad \text{as} \quad \epsilon \to 0 \quad \text{for fixed} \quad \theta \neq 0$$

and Γ satisfies the outer boundary conditions

$$\Gamma(\pi) = 0, \quad \Gamma(0) = \Gamma''(0) = 0$$

for symmetric modes, or $\quad \Gamma(\pi) = 0, \quad \Gamma'(0) = \Gamma'''(0) = 0$

for antisymmetric modes, to leading order. We have found the two solutions

$$\Gamma_0(\theta) = \tfrac{1}{2}(1 + \cos\theta) \quad \text{corresponding to} \quad s = -1$$

and $\Gamma_0(\theta) = \frac{1}{2}\{(1-\cos\theta)\ln\frac{1}{2}(1-\cos\theta) + (1+\cos\theta)\}$ corresponding to $s = 1$. Note that both represent antisymmetric modes. Further, we assume inner representations $G(y,R) = \gamma(\xi,\epsilon)$, where

$$\gamma(\xi,\epsilon) = \gamma_0(\xi) + \epsilon\gamma_1(\xi) + \ldots \quad \text{when} \quad s = -1$$

and

$$\gamma(\xi,\epsilon) = \gamma_0(\xi) + \epsilon\ln\epsilon\gamma_1(\xi) + \ldots \quad \text{when} \quad s = 1.$$

Solving and matching, we find

$$\gamma_0 = 1, \quad \gamma_1 = -\tfrac{1}{4}\xi^2 \quad \text{for} \quad s = -1$$

and

$$\gamma_0 = 1, \quad \gamma_1 = -\tfrac{1}{4}\xi^2 \quad \text{for} \quad s = 1.$$

Comparison with numerical results leads us to identify $s = -1$ with the eigenvalue q_1 corresponding to the first antisymmetric mode, and $s = 1$ with q_2. Moreover, for the first antisymmetric eigensolution the asymptotic result predicts $G''(0) \approx -\frac{1}{2}\pi^2$, $G''(1) \approx \frac{1}{2}\pi^2 = 4.93480$, whereas numerical integration produces $G''(0) = -4.86238$,

$G''(1) = 4.96298$ and the eigenvalue -0.99527 at $R = -2000$; there is good agreement for other properties also. For the second antisymmetric eigensolution the asymptotic results predict $G''(0) \approx \frac{1}{2}\pi^2 \ln(-\pi R^{-1})$ and $G''(1) \approx 0$; at $R = -2000$ the former result becomes $G''(0) \approx -31.85994$ whilst numerical integration yields $G''(0) = -29.76432$, $G''(1) = -0.01854$ and an eigenvalue of 1.00700; there is again good agreement for other properties.

3. Numerical results

For $\chi = 0$ many numerical results have been presented by ZDB, and in this section we confine attention to the case $\chi = 1$. We have computed solutions of the eigenvalue problem consisting of (1.15) and the boundary conditions $\mathbf{B}_A G = \mathbf{0}$ and $\mathbf{B}_S G = \mathbf{0}$, which correspond to antisymmetric and symmetric modes respectively. As a consequence of our results we next proceed to calculations of asymmetric steady solutions of (1.8) subject to (1.9). In all these calculations we have made use of a standard computer procedure to integrate the two-point boundary-value problem with ordinary differential equations for both the basic flow F and the eigenfunction G; the shooting method was used and the normalization for the eigenfunction was set as $G'' = 1$ at $y = -1$. Certain difficulties were encountered in the computations for some flows – these will be mentioned as they occur in the text.

We started the tabulations at $|R| \ll 1$, taking advantage of the known analytical results of §2.1, and proceeded to larger values of R. For $R = 0.1$ our numerical procedure yielded $q_1 = -98.96046$, $r_1 = -201.56805$, $q_2 = -394.85170$, $r_2 = -596.68052$, whereas the first two terms of the small-R expansions of (2.4) and (2.5) with $\chi = 1$ give rise to values of -98.96202, -201.56683, -394.85068, -596.67968 respectively, thus showing good agreement. This tabulation of eigenvalues for the type I solutions was continued for larger values of $|R|$; we present the results in figure 2.

We describe first the case when $R > 0$, noting that the eigenvalue q_1 increases through zero at $R = R_1$, where $R_1 = 132.75849$. This indicates a change in the symmetric solutions of type I – they are temporally unstable for $R > R_1$. It also appears that $q_1 \downarrow 0$ and $r_1, q_2, r_2 \uparrow 0$ as $R \to \infty$ and we recall that the asymptotic results of §2 predicted that all the eigenvalues approach zero as $R \to \infty$.

The change of sign of q_1 at R_1 suggests the existence of asymmetric solutions in the vicinity of R_1. We have therefore investigated the occurrence of asymmetric solutions of (1.8) subject to (1.9) in the neighbourhood of R_1: we denote the types of these solutions by I_1 and I_1' (the mirror image of I_1 in the centreline of the channel). The results are presented in figure 3(*b*) and they show the asymmetric solutions forming two branches of a pitchfork bifurcation. The tabulation of the asymmetric solutions was continued to large values (≈ 7500) of R; asymptotic properties of these solutions will be discussed in §5.

We also evaluated the eigenvalues corresponding to asymmetric solutions for $R > R_1$ and these are shown in figure 4. Note that since the primary flow is asymmetric the modes are neither symmetric nor antisymmetric but we continue to use the same label (q_n or r_n) for the eigenvalue for $R > R_1$ as for $R < R_1$. Our numerical results exhibit the familiar property that X, the slope of $q_1(R)$ as $R \uparrow R_1$ is related to Y, the slope of $q_1(R)$ as $R \downarrow R_1$, by the equation $Y = -2X$ (see Banks, Drazin & Zaturska 1988).

Moreover we observe that q_1 and r_1 coalesce at $R = 146.8$; for R close to, but greater than, 146.8 we find a complex conjugate pair of eigenvalues with negative

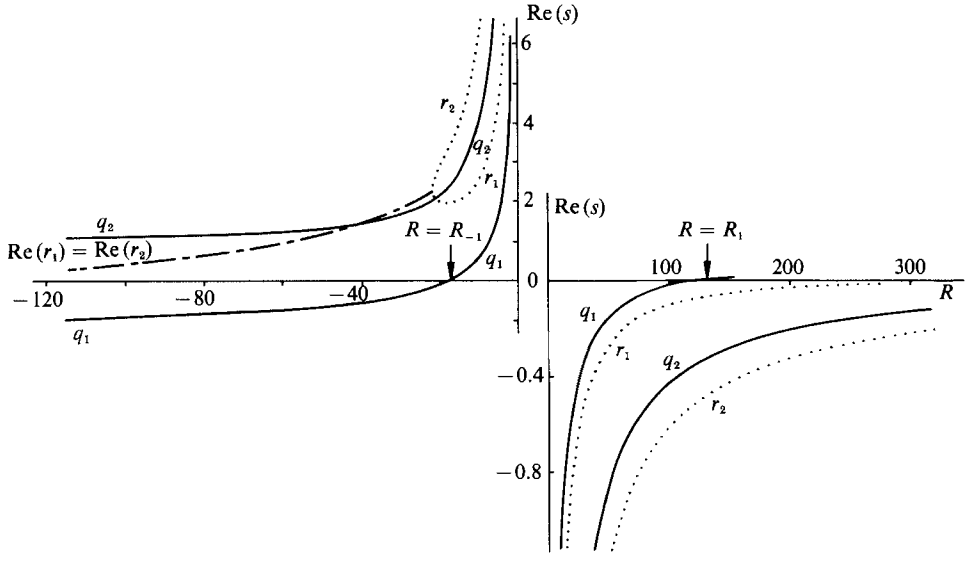

FIGURE 2. Some antisymmetric (q_n) and symmetric (r_n) eigenvalues for type I symmetric solutions with $\chi = 1$. The full curves represent the real antisymmetric eigenvalues, the dotted curves represent the real symmetric eigenvalues, and the chain curves represent the real part of the complex symmetric eigenvalues. Note the different scales for $R > 0$ and $R < 0$.

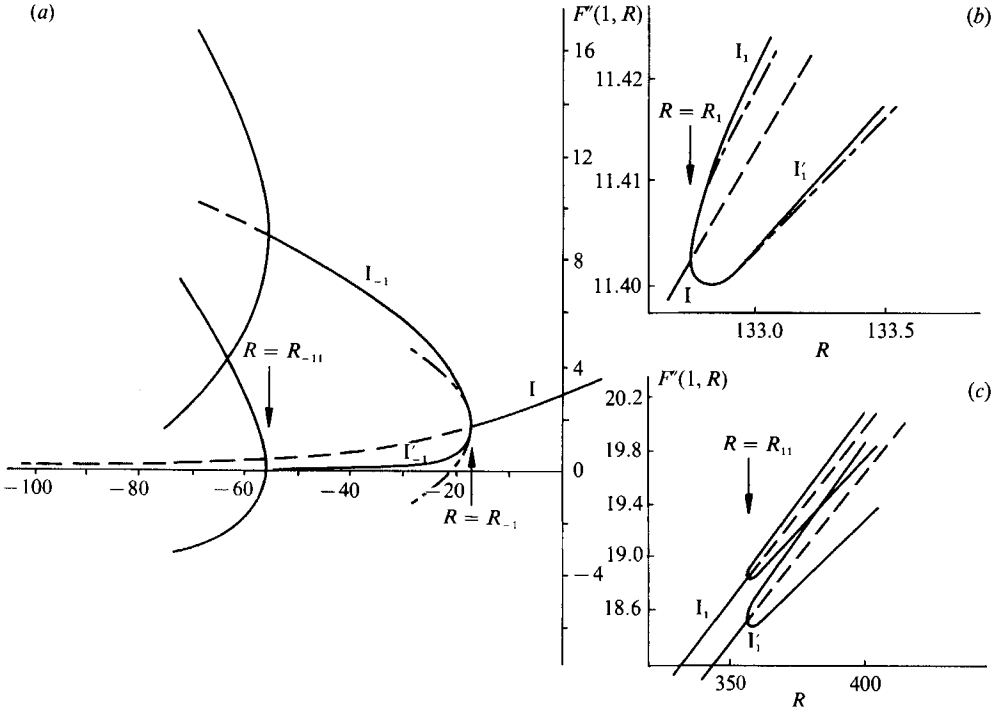

FIGURE 3. The full curves represent stable steady, periodic or quasi-periodic solutions, the dashed curves unstable solutions and the chain curves represent the first three terms of the asymptotic results of §4. Values of $F''(1, R)$ corresponding to $\chi = 1$ for (*a*) the symmetric solutions I, the asymmetric solutions I_{-1} and I'_{-1} and the periodic solutions, (*b*) the symmetric solutions I and the asymmetric solutions I_1 and I'_1, and (*c*) the asymmetric solutions I_1 and I'_1 and the periodic solutions.

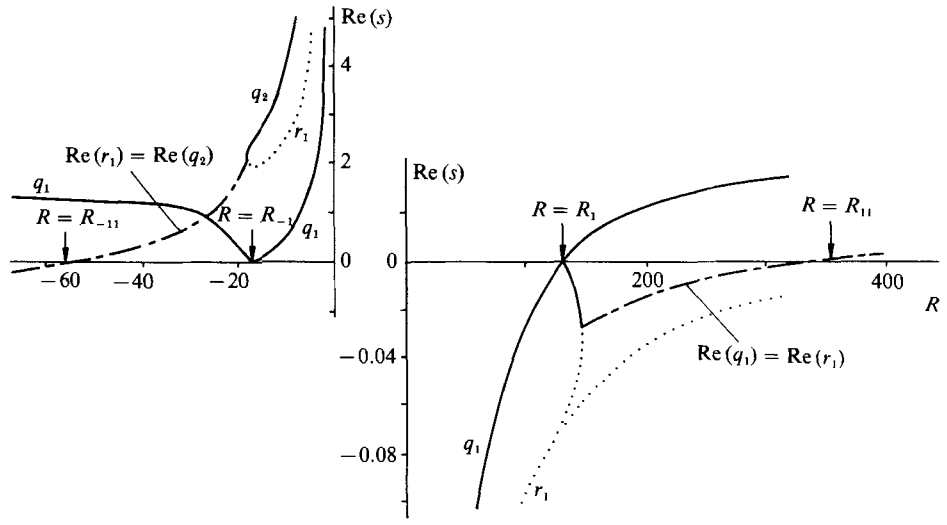

FIGURE 4. Some eigenvalues for symmetric solutions I and for asymmetric solutions I_1, I'_1, I_{-1} and I'_{-1}. The full curves represent the real eigenvalues q_n, the dotted curves represent the real eigenvalues r_n and the chain curves represent the real part of the complex eigenvalues. Note the different scales for $R > 0$ and $R < 0$.

real part. As R increases further this real part increases, eventually vanishing at $R = R_{11}$, where $R_{11} = 355.5738$ and becoming positive for $R > R_{11}$. This zero in the real part indicates the existence of a Hopf bifurcation – the asymmetric solutions on this branch cease to be temporally stable and periodic asymmetric solutions appear for $R > R_{11}$. The details of the Hopf bifurcation are presented in §4 and we shall return to such periodic solutions again in §7. On further increasing R we find that the pair of complex conjugate eigenvalues again become real on the I_1 (or I'_1) branch, this occurring at a Reynolds number of about 4.08×10^3.

We now turn our attention to the calculations corresponding to type I solutions for $R < 0$ and note (see figure 2) that here too there is a change in the sign of q_1, which occurs at $R = R_{-1}$, where $R_{-1} = -17.30715$, again leading to a change in the temporal stability of the symmetric solutions. Thus, solutions of type I are temporally stable only in the range $R_{-1} < R < R_1$. On decreasing R below R_{-1} we find that the eigenvalues r_1 and r_2 coalesce at $R \approx -21.7$; for R close to, but less than, this value we find a complex conjugate pair of eigenvalues with positive real part which appears to decrease as R decreases. The real eigenvalues q_1 and q_2 also decrease with decreasing R and appear to approach -1 and 1 respectively, values that are consistent with the asymptotic results presented in §2. Further, we find that $\mathrm{Re}\,(r_1)$ $(= \mathrm{Re}\,(r_2))$ vanishes at $R \approx -170$, which suggests that an unstable symmetric periodic solution originates here at a Hopf bifurcation. We refer in §7 to the possible consequences of this.

From the change of sign of q_1 at R_{-1} we again inferred the existence of asymmetric solutions in the neighbourhood of R_{-1}. We therefore sought asymmetric solutions of (1.8) subject to (1.9) in the vicinity of R_{-1} – we name the types of these solutions I_{-1} and I'_{-1} (the mirror image of I_{-1} in the centreline of the channel) by analogy with the notation for positive R; they are shown in figure 3(*a*). Some care was required regarding the direction of integration in computation of these asymmetric solutions, and, indeed, also in that of symmetric solutions for 'large' negative values of R.

The tabulation of the eigenvalues q_1, r_1, q_2 was continued into the region $R < R_{-1}$ for the asymmetric solutions I_{-1}, I'_{-1} and the results are shown in figure 4 – here too the modes are neither symmetric nor antisymmetric and the usual relationship $Y = -2X$ holds between the slope X of $q_1(R)$ as $R \downarrow R_{-1}$ and the slope Y of $q_1(R)$ as $R \uparrow R_{-1}$. We note also that the eigenvalue q_1 corresponding to asymmetric basic flows increases monotonically as R decreases beyond R_{-1}.

However, for these asymmetric basic flows it is r_1 and q_2 that coalesce, at $R = -17.46$, and for R close to, but less than, this value there is a complex conjugate pair of eigenvalues with positive real part. With a further decrease in Reynolds number this real part decreases, so that these complex eigenvalues become the principal eigenvalues, and eventually vanishes at $R = R_{-11}$, where $R_{-11} = -55.77$; for $R < R_{-11}$ this real part is negative. The change of sign of the real part of the eigenvalues at $R = R_{-11}$ corresponds to a Hopf bifurcation, and indicates the end of the temporally stable asymmetric solutions on this branch and the start of periodic asymmetric solutions. Some details of the Hopf bifurcation are given in §4 and of the periodic solutions in §7.

4. Local bifurcation theory

We now consider perturbations of a steady solution to examine the bifurcations that occur. Thus we suppose that $F = F_0$ is a solution of the system (1.8), (1.9) when $R = R_0$ and seek to perturb this solution for small $\epsilon = R - R_0$. It is well known that a series in powers of ϵ is appropriate at a regular point but in powers of $\epsilon^{\frac{1}{2}}$ at a turning point or at a pitchfork bifurcation. Accordingly, assume the expansion

$$F(y, R) = F_0(y) + \epsilon^{\frac{1}{2}} F_{\frac{1}{2}}(y) + \epsilon F_1(y) + \ldots \quad \text{as} \quad \epsilon \to 0 \tag{4.1}$$

and substitute it into the problem (1.8), (1.9). Equating coefficients of terms in ϵ^0 determines F_0. Recall that if F_0 represents a symmetric flow then it is an odd function.

Next we equate coefficients of $\epsilon^{\frac{1}{2}}$ and find that

$$\mathrm{L}F_{\frac{1}{2}} = 0, \quad \mathbf{B}F_{\frac{1}{2}} = \mathbf{0}, \tag{4.2}$$

where we define the linear differential operator L by

$$\mathrm{L}u = u^{\mathrm{iv}} + R_0(F_0 u''' - F'_0 u'' - F''_0 u' + F'''_0 u) \tag{4.3}$$

for all well-behaved functions u.

Comparison of system (4.2) with (1.15), (1.16) immediately leads to the conclusion that at a regular point, where $s \neq 0$ for all eigenvalues, the null function $F_{\frac{1}{2}} = 0$ is the only solution. Indeed, it is readily shown that at such a point the perturbed solution is expressible as a series in integral powers of ϵ and is unique, and that there is no bifurcation. So, in this weakly nonlinear analysis of bifurcations of steady solutions, let us suppose that $s = 0$. It follows, by the Fredholm alternative, that F is not unique when R is near R_0; for system (4.2) has solution

$$F_{\frac{1}{2}} = aG, \tag{4.4}$$

where a is a constant which is arbitrary at this stage but will be determined later.

Proceeding to terms in ϵ^1 in system (1.8), (1.9), substituting for $F_{\frac{1}{2}}$, and applying a solvability condition (see ZDB for the details) we find at length that

$$J_1 + a^2 R_0 J_2 = 0, \tag{4.5}$$

where $$J_1 = \int_{-1}^{1} G^\dagger(F_0' F_0'' - F_0 F_0''')\,\mathrm{d}y, \quad J_2 = \int_{-1}^{1} G^\dagger(G'G'' - GG''')\,\mathrm{d}y,$$

the adjoint eigenfunction $G^\dagger$ satisfies

$$\mathrm{L}^\dagger G^\dagger = 0, \quad \mathbf{B}G^\dagger = \mathbf{0}, \tag{4.6}$$

and the adjoint operator $\mathrm{L}^\dagger$ is defined by

$$\mathrm{L}^\dagger u = u^{\mathrm{iv}} - R_0(F_0 u''' + 4F_0' u'' + 4F_0'' u'). \tag{4.7}$$

(Note that non-trivial $G^\dagger$ exists because $s = 0$.) Equation (4.5) determines a provided that the second integral does not vanish. Various cases arise according to whether certain integrals vanish or not. We distinguish the two cases which arise in the present problem.

(i) $s = 0$, $J_1 \neq 0$ and $J_2 \neq 0$. In this case F has a power series in $\pm(\epsilon \operatorname{sgn} a^2)^{\frac{1}{2}}$ giving two solutions for R near R_0 if $R > R_0$ and none if $R < R_0$ when $a^2 > 0$ and giving two solutions if $R < R_0$ and none if $R > R_0$ when $a^2 < 0$ respectively. The bifurcation at $R = R_0$ is thus a turning point.

(ii) $s = 0$, $J_1 = 0$ and $J_2 = 0$. In this case it may be shown (cf. ZDB) that $a = 0$ or

$$a^2 = \frac{\displaystyle\int_{-1}^{1} G^\dagger\{F_0 G''' - F_0' G'' - F_0'' G' + F_0''' G + R_0(GH''' - G'H'' - G''H' + G'''H)\}\,\mathrm{d}y}{\displaystyle R_0^2 \int_{-1}^{1} G^\dagger(GK''' - G'K'' - G''K' + G'''K)\,\mathrm{d}y}, \tag{4.8}$$

where the functions H and K are defined by the problems

$$\mathrm{L}H = F_0' F_0'' - F_0 F_0''', \quad \mathbf{B}H = \mathbf{0}, \tag{4.9}$$

and

$$\mathrm{L}K = G'G'' - GG''', \quad \mathbf{B}K = \mathbf{0}. \tag{4.10}$$

If F_0 corresponds to a symmetric flow of type I then the root $a = 0$ corresponds to the continuation of the same flow and the other two roots to asymmetric flows; F has an expansion in powers of $\pm(\epsilon \operatorname{sgn} a^2)^{\frac{1}{2}}$ so that there are three solutions F for R near R_0 if $R > R_0$ and one if $R < R_0$ when $a^2 > 0$, and vice versa when $a^2 < 0$. The symmetry of the problem in $\pm y$ shows that this pitchfork bifurcation will in general arise if F_0 is an odd function and G and $G^\dagger$ are even functions.

In summary, we expect bifurcation of steady solutions according to cases (i), (ii) when the principle of exchange of stabilities is valid, i.e. when $s = 0$ at linear marginal stability. We may expect a Hopf bifurcation there otherwise, i.e. if $s = \pm \mathrm{i}\omega_0$ at $R = R_0$ for some $\omega_0 > 0$. Before we proceed to investigate the latter case, however, note that at $R = R_1$ or R_{-1}, where $q_1 = 0$, the conditions of (ii) hold because both G and $G^\dagger$ are even functions, and so there is a pitchfork bifurcation. Since $r_1 \to 0$ as $R \to \infty$ for solutions of type I, we anticipate a turning point at $R_2 = \infty$ which leads to symmetric solutions of type II. We infer from Brady & Acrivos (1981) that at $R = R_3$, where $r_1 = 0$, the conditions of (i) hold because both G and $G^\dagger$ are odd functions, and hence there is a turning point which we interpret as marking the boundary between flows of types II and III (although Brady & Acrivos distinguished those types by a change of flow direction at the centre of the channel). These bifurcations are all located in figure 1.

Numerical calculations for asymmetric steady basic flows indicate that, as R increases through R_{11} or decreases through R_{-11}, $\mathrm{Re}(s)$ increases or decreases through

zero respectively: so we now investigate the possibility of a Hopf bifurcation at such a point, where $s = \pm i\omega_0$. Suppose that the two eigenfunctions G, G^* correspond to the eigenvalues $i\omega_0$ and $-i\omega_0$ respectively, where we use an asterisk to denote the complex conjugate. Then seek weakly nonlinear solutions of period $2\pi/\omega$ for small $\epsilon = R - R_0$, expanding

$$f(y,\tau,R) = F_0(y) + \epsilon^{\frac{1}{2}} f_{\frac{1}{2}}(y,\tau) + \epsilon f_1(y,\tau) + \dots \tag{4.11}$$

and

$$\omega = \omega_0 + \epsilon^{\frac{1}{2}}\omega_{\frac{1}{2}} + \epsilon\omega_1 + \dots \quad \text{as} \quad \epsilon \to 0, \tag{4.12}$$

where

$$f(y,\tau+2\pi,R) = f(y,\tau,R) \quad \text{for all} \quad \tau = \omega t.$$

We next substitute (4.11) and (4.12) into (1.5) and boundary conditions (1.6). Note that, because the basic flow is asymmetric, F_0 is neither odd nor even here. At length, we find that

$$\omega_{\frac{1}{2}} = 0 \tag{4.13}$$

and

$$f_{\frac{1}{2}}(y,\tau) = AG(y)\,e^{i\tau} + A^*G^*(y)\,e^{-i\tau}, \tag{4.14}$$

where

$$\begin{aligned} 0 = {} & i(\omega_0 + \omega_1 R_0)\int_{-1}^{1} G''g^\dagger\,dy - \int_{-1}^{1} g^\dagger(F_0 G'''' - F_0' G'' - F_0'' G' + F_0'''' G)\,dy \\ & - R_0\int_{-1}^{1} g^\dagger(GH'''' - G'H''' - G''H'' + G''''H)\,dy \\ & - R_0|A|^2\int_{-1}^{1} g^\dagger(Gg_1'''' - G'g_1''' - G''g_1'' + G''''g_1 + G^*k_1'''' - G^{*\prime}k_1''' - G^{*\prime\prime}k_1'' + G^{*\prime\prime\prime\prime}k_1)\,dy, \end{aligned} \tag{4.15}$$

$g^\dagger$, g_1 and k_1 are defined by

$$Lg^\dagger = i\omega_0 R_0 g^{\dagger\prime\prime}, \quad \mathbf{B}g^\dagger = \mathbf{0}, \tag{4.16}$$

$$Lg_1 = -R_0(G''''G^* - G''G^{*\prime} - G'G^{*\prime\prime} + GG^{*\prime\prime\prime\prime}), \quad \mathbf{B}g_1 = \mathbf{0}, \tag{4.17}$$

$$(L - 2i\omega_0 R_0\,d^2/dy^2)k_1 = -R_0(GG'''' - G'G''), \quad \mathbf{B}k_1 = \mathbf{0}, \tag{4.18}$$

and H by a problem of the form (4.9). The upshot of this calculation is that the complex equation (4.15) gives two real equations to determine $|A|^2$, the square of the amplitude of $f_{\frac{1}{2}}$, and ω_1, which gives the leading approximation to the change of the frequency of the periodic solution for small ϵ.

We have evaluated the various integrals met in these perturbations about some bifurcation points. At the pitchfork bifurcation with $R_0 = R_1$ we find from (4.8) that the non-zero values of a are ± 0.017361. This shows that the pitchfork is supercritical, because $a^2 > 0$, and also agrees well with direct numerical integrations of asymmetric solutions F for small $R - R_1 > 0$. For $R_0 = R_{-1}$, we have similarly found $a = \pm 0.89932i$ so that the pitchfork is subcritical and again agrees with the direct numerical calculations of asymmetric solutions near $R = R_{-1}$.

With $R_0 = R_{11}$, corresponding to the Hopf bifurcation of the solutions of type I_1 (or I_1'), where $s = \pm 0.035577i$, we have evaluated the integrals in (4.15) and obtained $|A|^2 = 0.000573$ and $\omega_1 = 0.000305$. We have used these results in figure 3(*c*) to sketch the behaviour of the periodic solutions that emanate at $R = R_{11}$. With $R_0 = R_{-11}$ we attempted a straightforward numerical integration of the necessary equations but it appears that parasitic growth in the calculation for $G^\dagger$ precluded an accurate solution: in view of the detailed results and comparisons given in ZDB and the results at $R_0 = R_{11}$ we did not proceed further.

In the analysis above we have assumed symmetric boundary conditions (1.9) for F at $y = \pm 1$. In order to unfold the pitchfork bifurcations corresponding to $\chi = 1$ we consider (1.5) subject to the modified boundary conditions

$$\mathbf{B}f = [0, 1+\epsilon^{\frac{3}{2}}(k-l), 0, 1+\epsilon^{\frac{3}{2}}(k+l)]^{\mathrm{T}}, \tag{4.19}$$

where k and l are constants and $\epsilon = R - R_0$. We regard the system with $\epsilon = 0$, and so with symmetric boundary conditions, as 'perfect', and consider small imperfections which render the boundary conditions asymmetric when $l\epsilon^{\frac{3}{2}} \neq 0$. We define a 'slow' time $T = \epsilon t$ and write $f = F_0 + \epsilon^{\frac{1}{2}} f_{\frac{1}{2}} + \epsilon f_1 + \ldots$ as $\epsilon \to 0$. Then it is readily shown that

$$f_{\frac{1}{2}}(y, T) = A(T)\, G(y),$$

where
$$\frac{\mathrm{d}A}{\mathrm{d}T} = a_1 l + a_2 A + a_3 A^3,$$

$$a_1 = 2G^{\dagger\prime\prime\prime}(1)/R_0 \int_{-1}^{1} G^{\dagger} G''\, \mathrm{d}y, \quad a_2 = -a^2 a_3,$$

$$a_3 = R_0 \int_{-1}^{1} G^{\dagger}(GK''' - G'K'' - G''K' + G'''K)\, \mathrm{d}y \Big/ \int_{-1}^{1} G^{\dagger} G''\, \mathrm{d}y$$

and a^2 is given by (4.8). Thus, the steady solutions with symmetry breaking are governed by the cubic equation

$$a_3 A^3 + a_2 A + a_1 l = 0 \tag{4.20}$$

and the pitchfork bifurcation of the perfect system with $l = 0$ is unfolded into a primary and a secondary flow when $l \neq 0$.

We have numerically solved (1.8) subject to (4.19) when $l = k = -\Theta/2\epsilon^{\frac{3}{2}}$, taking $\Theta = 0.0001$ at $R = R_1$ and $\Theta = 0.01$ at $R = R_{-1}$. From (4.20) we infer that

$$\{F''(1) - F_0''(1)\}^3 - a^2\{G''(-1)\}^2 (R - R_0)\{F''(1) - F_0''(1)\}$$
$$- \Theta G^{\dagger\prime\prime\prime}(1)\{G''(-1)\}^3/R_0^2 \int_{-1}^{1} G^{\dagger}(GK''' - G'K'' - G''K' + G'''K)\, \mathrm{d}y = 0 \tag{4.21}$$

and this is confirmed by the numerical results shown in figure 5.

We next examine the perturbation of the pitchfork as χ varies. Suppose that at $\chi = \chi_0$ there is a pitchfork bifurcation at $R = R_0$, i.e. $s = 0$,

$$\int_{-1}^{1} G^{\dagger}(F_0 F_0''' - F_0' F_0'')\, \mathrm{d}y = 0, \quad \int_{-1}^{1} G^{\dagger}(GG''' - G'G'')\mathrm{d}y = 0.$$

Then we assume that the perturbation to χ is given by

$$\chi = \chi_0 + \epsilon\chi_1 + \epsilon^2\chi_2 + \ldots$$

and to G by
$$G = G_0 + \epsilon^{\frac{1}{2}} G_{\frac{1}{2}} + \epsilon G_1 + \ldots \quad \text{as} \quad \epsilon \to 0,$$

where G satisfies the eigenvalue problem (1.15) with $s = 0$, subject to (1.16), F is given by (4.1) and satisfies the system (1.8), (1.9) and $R = R_0 + \epsilon$. Using arguments similar to those in the earlier part of this section, we find at length that

$$\chi_1 = -\frac{\displaystyle\int_{-1}^{1} G^{\dagger}\{F_0 G_0''' - F_0' G_0'' - F_0'' G_0' + F_0''' G_0 + R_0(G_0 H''' - G_0' H'' - G_0'' H' + G_0''' H)\}\, \mathrm{d}y}{\displaystyle R_0 \int_{-1}^{1} G^{\dagger}(G_0 J''' - G_0' J'' - G_0'' J' + G_0''' J)\, \mathrm{d}y}, \tag{4.22}$$

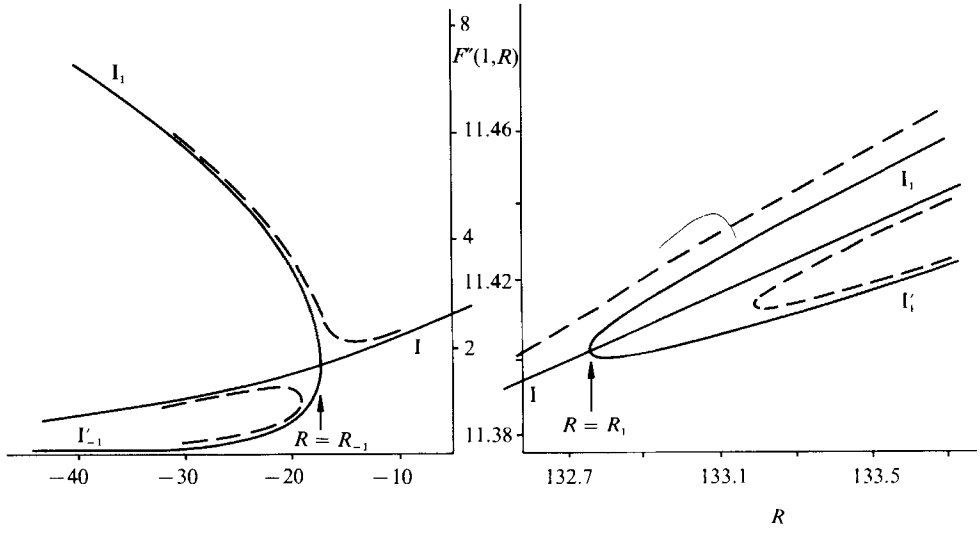

FIGURE 5. Values of $F''(1,R)$ for the solutions I, I_1 I'_1, I_{-1} and I'_{-1} at $\chi = 1$ represented by a full curve. The dashed curves indicate values when $\Theta = 0.0001$ for $R > 0$ and $\Theta = 0.01$ for $R < 0$ (see (4.21)) and show the unfolding of the pitchforks.

where J satisfies

$$\mathbf{L}J = 0, \quad \mathbf{B}J = [-1, 1, 1, 1]^{\mathrm{T}}. \tag{4.23}$$

Using (4.22), we found $\chi_1 = 0.0005855$ and 0.011546 for the pitchforks at R_1 and R_{-1} respectively. Further, for the pitchfork bifurcation at $\chi = 0$, $R = R_1 = 6.001353$ (see ZDB), we found $\chi_1 = 0.133945$.

Moreover, the locus of the pitchfork bifurcations in the (χ, R)-plane can be traced directly by numerically solving system (1.8), (1.9) concurrently with the system (1.15), (1.16) with $s = q_1 = 0$. The resulting curve is shown in figure 6 as are the slopes (at $\chi = 0, 1$) which have been found using the values of χ_1 obtained from (4.22). There is excellent agreement between the two sets of results. We also note that the values of $R_{\pm 1}$ obtained here for large $|\chi|$ agree well with the asymptotic result of the Appendix that $R_{\pm 1} \sim -4.5118\chi^{-1}$ as $\chi \to \mp\infty$.

The unfolding of the pitchfork bifurcations at $R = R_1$ and $R = R_{-1}$ for $\chi = 1$ together with that for $\chi = 0$ (see ZDB) forms part of a more general picture. We note that the nature of the unfolding for these two values with positive Reynolds number is the same, and we use this to present qualitatively, in figure 7, the unfolding for general values of χ.

5. Asymptotic results for asymmetric steady basic flows for large R

In the previous two sections we have established that asymmetric flows originate at the two pitchfork bifurcations, where $R = R_1$, R_{-1}. We now examine the asymptotic behaviour of these flows for large values of $|R|$ and $\chi = 1$.

When $R \gg 1$ the steady asymmetric flows have boundary layers with thickness of

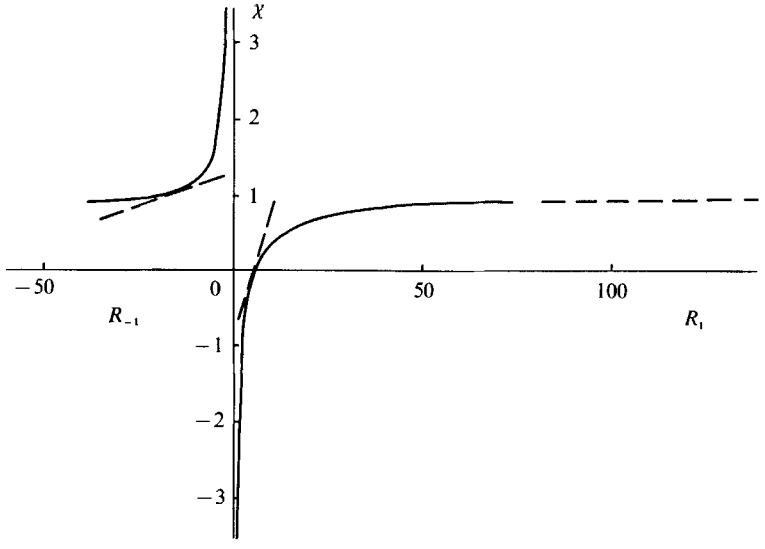

FIGURE 6. The values of the Reynolds number corresponding to pitchfork bifurcations for various values of χ. The dashed lines represent the asymptotic result (4.22) and correspond to the slope of the curve.

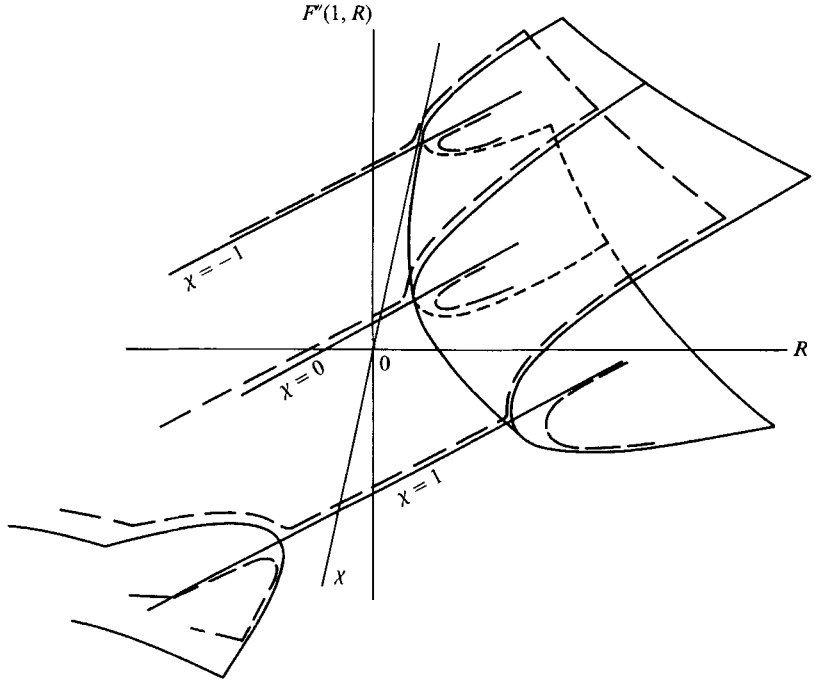

FIGURE 7. Perspective sketch of the values of $F''(1, R)$ for various values of R, χ represented by full curves. The long-dashed curves show the unfolding of the pitchforks for various χ.

order of magnitude $R^{-\frac{1}{2}}$ near each wall and a weak inviscid core which is driven by the boundary-layer flows. Accordingly we assume inner solutions of the form

$$F(y,R) = R^{-\frac{1}{2}}\psi^+(z,R), \quad \text{where} \quad z = (1-y)R^{\frac{1}{2}} \tag{5.1}$$

and

$$F(y,R) = R^{-\frac{1}{2}}\phi^+(\eta,R), \quad \text{where} \quad \eta = (1+y)R^{\frac{1}{2}}, \tag{5.2}$$

and write

$$\psi^+(z,R) = \psi_0^+(z) + R^{-\frac{1}{2}}\psi_1^+(z) + \ldots, \tag{5.3}$$

$$\phi^+(\eta,R) = \phi_0^+(\eta) + R^{-\frac{1}{2}}\phi_1^+(\eta) + \ldots \quad \text{as} \quad R \to \infty. \tag{5.4}$$

The functions ψ^+ and ϕ^+ satisfy the boundary conditions

$$\psi^+(0) = \phi^+(0) = \psi^{+\prime}(0) + 1 = \phi^{+\prime}(0) - 1 = 0. \tag{5.5}$$

Because the flow in the inviscid core is weak we assume that $\psi^{+\prime}(z) \to 0$ as $z \to \infty$ and $\phi^{+\prime}(\eta) \to 0$ as $\eta \to \infty$. In the inviscid core, in order to match with the boundary layers, the solution is assumed to take the form

$$F(y,R) = R^{-\frac{1}{2}}\Phi(y,R), \tag{5.6}$$

where

$$\Phi(y,R) = \Phi_0(y) + R^{-\frac{1}{2}}\Phi_1(y) + \ldots \quad \text{as} \quad R \to \infty; \tag{5.7}$$

the boundary conditions are determined via the matching procedure.

We find that

$$\psi_0^+(z) = -1 + \mathrm{e}^{-z}, \tag{5.8}$$

$$\phi_0^+(\eta) = 1 - \mathrm{e}^{-\eta}, \tag{5.9}$$

so that the boundary conditions for Φ_0 are $\Phi_0(1) = -1$, $\Phi_0(-1) = 1$. Then we may solve for Φ_0 to obtain

$$\Phi_0(y) = C_0 \cos(\tfrac{1}{2}\pi y + \epsilon_0), \tag{5.10}$$

where

$$C_0 \sin\epsilon_0 = 1. \tag{5.11}$$

Proceeding to the next order in the inner expansions we find firstly that ψ_1^+ and ϕ_1^+ are the same function, and then, at length, that

$$\psi_1^+(z) = \frac{\pi C_0 \cos\epsilon_0}{8\mathrm{e}}\mathrm{e}^{-z}\int_0^z (1+\mathrm{e}^v)\left\{\int_0^v \exp\left(\int_0^u \frac{3+\mathrm{e}^{-x}}{1+\mathrm{e}^x}\,\mathrm{d}x\right)\mathrm{d}u\right\}\mathrm{d}v. \tag{5.12}$$

We note that the present analysis does not determine the values of the constants C_0 and ϵ_0 but merely demands that they satisfy the condition (5.11). Consequences of the analysis are that

$$F''(\pm 1) = R^{\frac{1}{2}}\left\{\pm 1 + R^{-\frac{1}{2}}\frac{\pi C_0 \cos\epsilon_0}{4\mathrm{e}} + o(R^{-\frac{1}{2}})\right\} \tag{5.13}$$

and

$$F'(0) = -\tfrac{1}{2}R^{-\frac{1}{2}}\pi C_0 \sin\epsilon_0 + o(R^{-\frac{1}{2}}) \quad \text{as} \quad R \to \infty. \tag{5.14}$$

We have evaluated $2\mathrm{e}\pi^{-1}\{F''(1) + F''(-1)\}$ and $-2R^{\frac{1}{2}}\pi^{-1}F'(0)$ using values obtained from the exact numerical integration of the system (1.8), (1.9) for some large values of R and, using the leading terms displayed in (5.13) and (5.14), calculated the values of C_0, ϵ_0 to which they correspond. We find that for $R = 6400$, $C_0 = 2.0312$ and $\epsilon_0 = 0.53869$, for $R = 7200$, $C_0 = 2.1008$ and $\epsilon_0 = 0.51753$, and for $R = 7240$, $C_0 = 2.1043$ and $\epsilon_0 = 0.51667$. We do not guarantee the accuracy of all the figures, and it is possible that $C_0 = 2$, $\epsilon_0 = \frac{1}{6}\pi = 0.52360$.

Having determined the analytic behaviour of the solutions of type I_1 for large R to the order shown, we proceed to investigate the associated eigenvalue problem as defined by (1.15) with boundary conditions (1.16).

We first integrate (1.15) to obtain

$$G''' + \gamma + R(FG'' - 2F'G' + F''G) = RsG', \tag{5.15}$$

where γ is the constant of integration. If we now replace $F(y, R)$ by its leading outer term $R^{-\frac{1}{2}}C_0 \cos(\frac{1}{2}\pi y + \epsilon_0)$ and neglect the viscous term G''', we obtain the equation

$$\cos\theta\Gamma'' + (2\sin\theta - \bar{\mu})\Gamma' - \cos\theta\Gamma = -4\gamma_0/\pi^2 C_0, \tag{5.16}$$

where $\bar{\mu} = 2R^{\frac{1}{2}}s/\pi C_0$, $\gamma_0 = \gamma R^{-\frac{1}{2}}$, $\theta = \frac{1}{2}\pi y + \epsilon_0$ and $\Gamma(\theta) = G(y)$. We may immediately conclude that if we find finite values for $\bar{\mu}$ then $s \to 0$ as $R \to \infty$ for *all* eigenvalues. Although we have not solved (5.16) in the general case we have obtained the solution

$$\Gamma(\theta) = \frac{2\gamma_0}{\pi^2 C_0 \cos\epsilon_0}\cos(\theta - \epsilon_0), \quad \bar{\mu} = 0, \tag{5.17}$$

which satisfies the outer boundary conditions $\Gamma(\frac{1}{2}\pi + \epsilon_0) = \Gamma(-\frac{1}{2}\pi + \epsilon_0) = 0$. A consequence of this solution is that $G'(0, R) = 0$ to leading order, a result which is confirmed by our numerical results, as indeed is the eigenvalue $\bar{\mu} = 0$. We have not continued the matching to high order.

When $-R \gg 1$ it is convenient to write $R = -\rho$. The steady asymmetric flows have boundary layers whose thickness is of order of magnitude $\rho^{-\frac{1}{2}}$ near each wall, and are inviscid elsewhere when ρ is large. We assume an outer solution of the form

$$F(y, R) = \Phi(y, \rho), \tag{5.18}$$

where $$\Phi(y, \rho) = \Phi_0(y) + \rho^{-\frac{1}{2}}\Phi_1(y) + \ldots \quad \text{as} \quad \rho \to \infty \quad \text{for fixed} \quad y \neq \pm 1, \tag{5.19}$$

and Φ satisfies the outer boundary conditions

$$\Phi(\pm 1) = 0 \tag{5.20}$$

to leading order. We also assume that there are inner solutions of the form

$$F(y, R) = \rho^{-\frac{1}{2}}\psi^-(z, \rho) \quad \text{where} \quad z = (1 - y)\rho^{\frac{1}{2}}, \tag{5.21}$$

$$\psi^-(z, \rho) = \psi_0^-(z) + \rho^{-\frac{1}{2}}\psi_1^-(z) + \ldots \quad \text{as} \quad \rho \to \infty \quad \text{for fixed} \quad z, \tag{5.22}$$

and ψ^- satisfies the inner boundary conditions

$$\psi^-(0) = 0, \quad \psi^{-\prime}(0) = -1, \tag{5.23}$$

and

$$F(y, R) = \rho^{-\frac{1}{2}}\phi^-(\eta, \rho), \quad \text{where} \quad \eta = (1 + y)\rho^{\frac{1}{2}}, \tag{5.24}$$

$$\phi^-(\eta, \rho) = \phi_0^-(\eta) + \rho^{-\frac{1}{2}}\phi_1^-(\eta) + \ldots \quad \text{as} \quad \rho \to \infty \quad \text{for fixed} \quad \eta \tag{5.25}$$

and ϕ^- satisfies the inner boundary conditions

$$\phi^-(0) = 0, \quad \phi^{-\prime}(0) = 1. \tag{5.26}$$

These inner and outer solutions are matched at the edges of the boundary layers. Solving at successive orders of approximation we find

$$\Phi_0(y) = -2\pi^{-1}\cos\tfrac{1}{2}\pi y, \tag{5.27}$$

$$\psi_0^-(z) = -z \tag{5.28}$$

and ϕ_0^- satisfies the differential equation

$$\phi_0^{-\prime\prime\prime} - \phi_0^-\phi_0^{-\prime\prime} + \phi_0^{-\prime 2} = 1 \tag{5.29}$$

subject to the boundary conditions $\phi_0^-(0) = \phi_0^{-\prime}(0) - 1 = 0$, $\phi_0^{-\prime}(\eta) \to -1$ as $\eta \to \infty$. The problem for ϕ_0^- has been solved numerically and it is found that

$$\phi_0^{-\prime\prime}(0) = -1.328817, \quad \phi_0^-(\eta) = -\eta + \delta + o(1) \quad \text{as} \quad \eta \to \infty, \tag{5.30}$$

where $\delta = 1.96612$. Continuing with the matching to higher order we obtain

$$\Phi_1(y) = -\tfrac{1}{2}\delta \sin \tfrac{1}{2}\pi y + \delta\pi^{-1}(\tfrac{1}{2}\pi y \sin \tfrac{1}{2}\pi y + \cos \tfrac{1}{2}\pi y), \tag{5.31}$$

$$\psi_1^- = \phi_1^- = 0. \tag{5.32}$$

Moreover, the next term in the outer expansion is $O(\rho^{-1} \ln \rho)$, and the next terms in the expansions for ψ^- and ϕ^- are also of the same order of magnitude, so that we write

$$\begin{aligned}
\Phi &= \Phi_0 + \rho^{-\frac{1}{2}}\Phi_1 + \rho^{-1}\ln\rho\,\Phi_{21} + \rho^{-1}\Phi_2 + \ldots, \\
\psi^- &= \psi_0^- + \rho^{-\frac{1}{2}}\psi_1^- + \rho^{-1}\ln\rho\,\psi_{21}^- + \rho^{-1}\psi_2^- + \ldots, \\
\phi^- &= \phi_0^- + \rho^{-\frac{1}{2}}\phi_1^- + \rho^{-1}\ln\rho\,\phi_{21}^- + \rho^{-1}\phi_2^- + \ldots \quad \text{as} \quad \rho \to \infty.
\end{aligned}$$

We find

$$\Phi_{21}(y) = A_{21}\sin \tfrac{1}{2}\pi y + B_{21}(\tfrac{1}{2}\pi y \sin \tfrac{1}{2}\pi y + \cos \tfrac{1}{2}\pi y), \tag{5.33}$$

$$\psi_{21}^-(z) = 0; \tag{5.34}$$

since ϕ_0^- is known only numerically, numerical integration is necessary to solve for ϕ_{21}^-. The constants A_{21} and B_{21} are related by $A_{21} + \frac{1}{2}\pi B_{21} + \frac{1}{4}\pi = 0$.

We have compared the predictions of these asymptotic results with those from exact numerical integration of the system (1.8), (1.9). The asymptotic results indicate that

$$F''(-1,\rho) = -1.328817\,\rho^{\frac{1}{2}} + \rho^{-\frac{1}{2}}\ln\rho\,\phi_{21}^{-\prime\prime}(0) + \rho^{-\frac{1}{2}}\phi_2^{-\prime\prime}(0) + \ldots, \tag{5.35}$$

$$F''(1,\rho) = \rho^{-\frac{1}{2}}\psi_2^{-\prime\prime}(0) + \ldots \quad \text{as} \quad \rho \to \infty. \tag{5.36}$$

Comparison with results from exact numerical integration with $\rho = 900$ and 1600 indicates that $\psi_2^{-\prime\prime}(0) = 0$. Moreover, when $\phi_{21}^{-\prime\prime}(0)$, $\phi_2^{-\prime\prime}(0)$ are evaluated by using exact numerical results for $\rho = 900$, 1600 and a truncated form of (5.35), we find that $\phi_{21}^{-\prime\prime}(0) = 0.16224$, $\phi_2^{-\prime\prime}(0) = 5.58705$. With these values we find that (5.35) predicts values of -66.352496 and -79.656378 for $F''(-1)$ at $\rho = 2500$, 3600 whereas exact numerical integration yields -66.352163 and -79.655661 respectively. We may also infer from the asymptotic form that

$$F(0) = -2\pi^{-1} + 0.625835\rho^{-\frac{1}{2}} + \rho^{-1}\ln\rho\,B_{21} + \rho^{-1}\Phi_2(0) + \ldots, \tag{5.37}$$

$$\begin{aligned}
(2/\pi)^2 F''(0) = {} & 2\pi^{-1} + 0.625835\rho^{-\frac{1}{2}} + \rho^{-1}\ln\rho\,B_{21} \\
& + \rho^{-1}(2/\pi)^2\Phi_2''(0) + \ldots \quad \text{as} \quad \rho \to \infty.
\end{aligned} \tag{5.38}$$

Using each of these forms with results from the exact numerical integration at $\rho =$ 900, 1600 to determine the coefficient B_{21}, we find excellent agreement. Thus the comparison of the asymptotic and numerical results gives conviction that the analysis is valid.

In order to investigate the eigenvalues corresponding to large negative R we replace F in (5.15) by its leading outer term $-2\pi^{-1}\cos \frac{1}{2}\pi y$ and neglect the viscous term G''' to obtain the equation

$$\cos\theta_- \Gamma_-'' + (s + 2\sin\theta_-)\Gamma_-' - \cos\theta_-\Gamma_- = 2\gamma/R\pi, \tag{5.39}$$

where $\theta_- = \frac{1}{2}\pi y$, $\Gamma_-(\theta_-) = G(y)$. We have found one solution that leads to

$$G(y) = -(\gamma/R\pi)\cos \tfrac{1}{2}\pi y,$$

which satisfies the outer boundary conditions and has corresponding eigenvalue $s = 0$. However, with the limited number of eigenvalues computed we have been unable to verify this analytic result.

6. Three-dimensional temporal stability

We next investigate the linear stability of accelerating-wall channel flows to three-dimensional disturbances with a view to determining whether such perturbations could destabilize a flow which is stable to two-dimensional disturbances. Write $\boldsymbol{u} = \boldsymbol{u}_0 + \boldsymbol{u}_1$, $p = p_0 + p_1$, where $\boldsymbol{u}_0 = (xF', -F, 0)$ and p_0 represents the unperturbed pressure, and linearize the momentum equation for small perturbations $\boldsymbol{u}_1$, p_1 to obtain

$$\frac{\partial \boldsymbol{u}_1}{\partial t} + \boldsymbol{u}_1 \cdot \nabla \boldsymbol{u}_0 + \boldsymbol{u}_0 \cdot \nabla \boldsymbol{u}_1 = -\nabla p_1 + R^{-1} \nabla^2 \boldsymbol{u}_1. \tag{6.1}$$

In order to satisfy continuity,

$$\nabla \cdot \boldsymbol{u}_1 = 0. \tag{6.2}$$

The boundary conditions are $\boldsymbol{u}_1 = (u_1, v_1, w_1) = \boldsymbol{0}$ at $y = \pm 1$. Now assume that the disturbance is of a similar form to the undisturbed flow, i.e. that

$$u_1 = x\bar{u}(y, z, t), \quad v_1 = \bar{v}(y, z, t), \quad w_1 = \bar{w}(y, z, t).$$

It follows from the momentum equation that $p_1 = x^2 \bar{p}_1(t) + \bar{p}_{11}(y, z, t)$ for some functions $\bar{p}_1$, $\bar{p}_{11}$. We next use the method of normal modes and write

$$(\bar{u}, \bar{v}, \bar{w}) = \mathrm{e}^{st + \mathrm{i}kz} (\hat{u}(y), \hat{v}(y), \hat{w}(y)).$$

The momentum equation requires that $\bar{p}_1(t) \equiv 0$ and $\bar{p}_{11}(y, z, t) = \mathrm{e}^{st + \mathrm{i}kz} \hat{p}(y)$ for some function $\hat{p}$. Note that since $\bar{p}_1$ is identically zero we are restricted to considering only antisymmetric perturbations of this form. With these assumptions the equations become

$$s\hat{u} + 2F'\hat{u} + F''\hat{v} - F\hat{u}' = R^{-1}(\hat{u}'' - k^2\hat{u}), \tag{6.3}$$

$$s\hat{v} - F'\hat{v} - F\hat{v}' = -\hat{p}' + R^{-1}(\hat{v}'' - k^2\hat{v}), \tag{6.4}$$

$$s\hat{w} - F\hat{w}' = -\mathrm{i}k\hat{p} + R^{-1}(\hat{w}'' - k^2\hat{w}), \tag{6.5}$$

$$\hat{u} + \hat{v}' + \mathrm{i}k\hat{w} = 0, \tag{6.6}$$

with boundary conditions

$$\hat{u}(\pm 1) = \hat{v}(\pm 1) = \hat{w}(\pm 1) = 0. \tag{6.7}$$

We examine first the case when $|R| \ll 1$ by writing $Rs = -\sigma$ and find that

$$\sigma \to k^2 + n^2\pi^2 \quad \text{as} \quad R \to 0 \quad \text{for} \quad n = 1, 2, \ldots.$$

Therefore, for all χ, if $|R| \ll 1$ then $\sigma > 0$ for all real k and so such channel flows are more stable to three-dimensional disturbances of similarity form than to two-dimensional ones.

For $R \gg 1$ a similar analysis to that in §2 leads to

$$q_n = \alpha(3 - 2n) - k^2 R^{-1} + o(R^{-1}) \quad \text{as} \quad R \to \infty \quad (n = 1, 2, \ldots)$$

indicating, when compared to (2.20), again that these three-dimensional disturbances are more stable than two-dimensional disturbances of the same form.

For $-R \gg 1$ a substitution of the appropriate asymptotic form for F into (6.3)–(6.6) does not lead to a decoupling of the system and therefore no simple conclusions may be drawn regarding the eigenvalues.

R	$F''(-1,R)$	$F''(1,R)$	t	$f_{yy}(-1,t,R)$	$f_{yy}(1,t,R)$
−55	−8.98923	0.04338	2400	−8.98904	0.04343
−50	−8.46170	0.05305	1200	−8.46151	0.05305
−35	−6.58247	0.11872	1200	−6.58239	0.11872
−30	−5.78651	0.17437	1200	−5.78644	0.17437
−25	−4.81344	0.28773	1200	−4.81341	0.28775
−20	−3.43568	0.60906	1200	−3.43564	0.60908
−18	−2.50516	1.02658	1200	−2.50513	1.02658
−17	−1.68782	1.68782	1200	−1.68782	1.68784
−10	−2.18149	2.18149	1200	−2.18151	2.18151
20	−4.71321	4.71321	600	−4.71321	4.71321
50	−6.95412	6.95412	600	−6.95415	6.95412
100	−9.85364	9.85364	600	−9.85356	9.85357
130	−11.27931	11.27931	600	−11.27909	11.27990
150	−12.16722	12.03330	600	−12.14817	12.13507
200	−14.06881	13.84533	600	−14.06806	13.84492
250	−15.74657	15.48190	600	−15.74502	15.48033
300	−17.26686	16.97406	600	−17.26786	16.97382
350	−1866655	18.35138	600	−18.66990	18.38888
			2400	−18.67277	18.35490

TABLE 1. Comparison of numerically calculated stable steady stolutions of the system (1.8), (1.9) with unsteady solutions of the system (1.5), (1.6) after quite long times of integration

7. Initial-value problem

We next return to the initial-value problem (1.5), (1.6) for $f(y, t, R)$ with an initial condition of the form $f(y, 0, R) = \hat{f}(y)$ for given R, where $\hat{f}$ is assumed to be well behaved and to satisfy boundary conditions (1.6). The case $\chi = 0$ has been considered by ZDB and we confine attention here to $\chi = 1$. We recall that when $\chi = 0$ the flow is driven by suction or injection and when $\chi = 1$ the flow is driven solely by the uniform acceleration of the channel walls.

In the numerical work of this section we have first taken $\hat{f}(y) = -\pi^{-1}(\operatorname{sgn} R)\sin \pi y$ for the initial condition, although, once a numerical solution was found for reasonably large values of t at a particular Reynolds number, the final result was taken as the initial condition at a neighbouring Reynolds number. We are interested here in the properties of 'developed' flow and have not specifically considered the development of the flow for various functions $\hat{f}$.

For the numerical integration of the nonlinear diffusion equation (1.5) we have used the same computer procedure (see Berzins & Dew 1989) as that used by ZDB. With specimen values of the Reynolds number we reproduced accurately, at finite values of t, the steady solutions, symmetric and asymmetric, that were discussed in §3. In table 1 we give detailed comparisons for $-55 \leqslant R \leqslant 350$ – we recall that for $R = R_{-11} - 0$ and for $R = R_{11} + 0$ our linear and weakly nonlinear results predict periodic flows, and further that for $R_{11} < R < R_{-1}$ and for $R_1 < R < R_{11}$ the stable

steady flows are asymmetric. It will be noted from the table that in most cases the time of integration was not long enough to achieve convergence to a steady solution. It should also be noted that, in spite of the success of these tests, the computer procedure was designed for general use, not to solve our particular problem. So some of our numerical results for chaotic solutions, which are notoriously difficult to compute accurately, may not be as accurate as we would wish. However, we are confident of the qualitative results presented here.

From the numerical results of this section it is possible to detect, for $R_1 < R < R_{11}$ and $R_{-11} < R < R_{-1}$, the oscillatory behaviour of $f_{yy}(1, t, R)$ as t increases with R fixed, and, for $R_{-1} < R < R_1$ the monotonic behaviour – all of which is consistent with the eigenvalue results reported in §3.

We have continued the calculations for values R at which we expect periodic solutions and have also proceeded to values beyond. It will be convenient to discuss the cases when $R < R_{-11}$ and $R > R_{11}$ separately in the two subsections that follow. We present only representative results obtained: we do this by plotting the phase plane of the state variables $f_{yy}(-1, t, R)$ and $f_{yy}(1, t, R)$ for the gross features and some Fourier spectra for the finer detail.

In interpreting the dynamics of the unsteady solutions it is helpful to regard each solution as an orbit in an infinite-dimensional phase space and examine the orbits geometrically. Each steady solution, of type I, I_1, I'_1, I_{-1}, I'_{-1}, II or III, is represented by a fixed point in that space for those values of R for which it exists; it is convenient to denote that point simply by I, I_1, I'_1, I_{-1}, I'_{-1}, II or III respectively. For the values of R of greatest interest, such a point (if it exists) is unstable and therefore a repellor, the neighbouring orbits being governed by the point's linear stability characteristics, which we have described earlier. For this reason it is important to recognize whether the fixed point is a saddle point, a saddle focus or a bifocus. Likewise each periodic solution is represented by a closed orbit in phase space, the orbit attracting or repelling neighbouring orbits according to whether the periodic solution is stable or unstable respectively. Glendinning (1988) has reviewed the geometrical theory of the onset of chaos after the breaking up of homoclinic orbits; in particular, he considered systems with the same symmetry as the system (1.5), (1.6). His review is the background to our geometrical interpretation of our numerical results.

7.1. $R > R_{11}$

The results of this subsection have certain properties in common with the results of ZDB. We begin by plotting $f_{yy}(1, t, R)$ versus $f_{yy}(-1, t, R)$ with $R = 357$ $(= R_{11} + 1.4264)$ for values of t between 2400 and 4400. The curve spirals outwards anticlockwise as t increases with no appearance of convergence – we presume that the Floquet exponent governing the approach to the periodic solution is complex with small, but negative, real part. This spiralling recurred with $R = 370$, but with $R = 400$ there was convergence to a periodic solution. This follows a similar pattern to that found by ZDB except that near the Hopf bifurcation the decay to the periodic solutions was much more rapid. With $R = 1200$ we find some remarkable changes in the phase plot as shown in figure 8(*a*). The most obvious feature is that the orbit has split into two, with the line of 'symmetry', $f_{yy}(1, t, R) + f_{yy}(-1, t, R) = 0$, being the common part: the orbit to the left of this line is traversed anticlockwise around the unstable asymmetric solution I'_1, and that to the right of the line is traversed clockwise around I_1. The points I_1, I'_1 are indicated by crosses, and the saddle point I by a plus sign. We note that the flow corresponding to a point in the phase diagram along the 'symmetry' line is indeed symmetric but not of type I. The Fourier

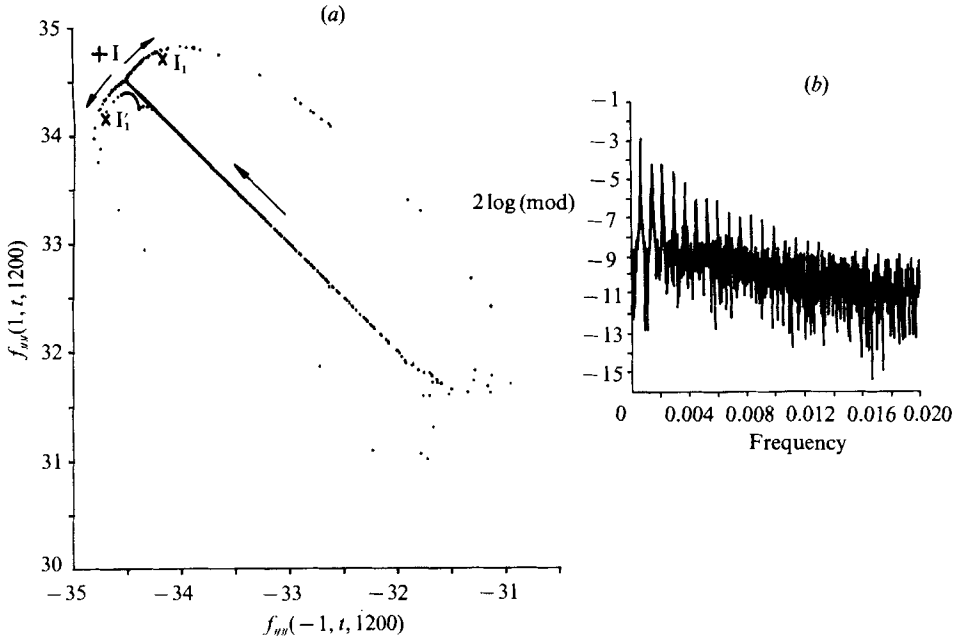

FIGURE 8. (*a*) Phase plane of $f_{yy}(1, t, 1200)$ and $f_{yy}(-1, t, 1200)$ with t as parameter. The unstable steady solutions I_1, I_1' are indicated by crosses, and I is indicated by a plus sign. (*b*) Logarithm (to the base 10) of the square of the modulus of the Fourier transform of time series of $f_{yy}(1, t, 1200)$ versus frequency.

spectrum and the phase plot indicate chaos. Another noteworthy feature is the appearance of a cusp near (−34.6, 34.3). The plot is taken from the integration starting at $t = 4000$ and ending at $t = 37000$, but this time interval was split into subintervals and the integration was restarted repeatedly. During integration over one subinterval this orbit involving the cusp was produced and could be reproduced on repeating the calculation, although the cusp could be eliminated by working to greater accuracy. We shall interpret this later.

For $R = R_{11} + 0$ we have found (from the results presented in §3) that the period of the motion is about 180. The period increases with R (see §4) and is about 250 at $R = 400$. With such large periods the determination of the frequency via the Fourier coefficients requires very long ranges of integration. We have contented ourselves here with showing in figure 8(*b*) the Fourier spectrum corresponding to $R = 1200$; the spectrum is further evidence for the existence of chaos.

So, to summarize the numerical results, we find for $R = R_{11} + 0$ evidence that the time series of state variables are sinuous and that as R increases the development of the flow is similar to that found by ZDB, resulting in chaos. However, in contrast to their results, the eigenvalues of type I flows all tend to zero as the Reynolds number tends to infinity (see §2), resulting in neutrally stable flows as $R \to \infty$. From the asymptotic analysis of §2 and the numerical results of §3 we infer that $-q_1/r_1 > 1$ for the solutions of type I when R is sufficiently large, and so the theory of Glendinning (1988) suggests that the onset of chaos follows the formation of two homoclinic orbits: as R increases beyond R_{11} the limit cycles that spring from I_1 and I_1' grow until they approach the solution I in such a way that their perturbations are proportional to the stable first symmetric eigenfunction G_2, i.e. approach in the

direction of G_2, and leave in the direction of the unstable first antisymmetric eigenfunction G_1.

It was found convenient by ZDB to express

$$f(y,t,R) = F^{(1)}(y,R) + X(t)\,G_1(y,R) + Y(t)\,G_2(y,R) + Z(t)\,G_3(y,R) \tag{7.1}$$

as a crude approximation, where $F^{(1)}$ is the solution I. This simple model explains many qualitative features of the dynamics. The limit cycles which lose stability persist, presumably, although their positions are unknown, and influence the orbits. We hypothesize that it is because of such unstable limit cycles that the cusp in figure 8(*a*) appears as the projection of a smooth orbit in a higher-dimensional space onto the phase plane.

We recall that we have calculated for the basic solutions I_1, I_1' only the first two eigenvalues (q_1 and r_1) and determined the position ($R = R_{11}$) at which $\mathrm{Re}\,(q_1)$ ($= \mathrm{Re}\,(r_1)$) vanishes so giving rise to a stable periodic solution at a Hopf bifurcation. We suspect that the third and fourth eigenvalues (q_2 and r_2) may coalesce and become complex, and the vanishing of their real part (at $R > R_{11}$) would imply that an unstable periodic solution originates at a Hopf bifurcation.

7.2. $R < R_{-11}$

We begin this subsection by plotting the phase plane of $f_{yy}(1,t,R)$ versus $f_{yy}(-1,t,R)$ in figure 9 for $R = -56$ ($\approx R_{-11} - 0.23$) and -70 with $1500 < t < 4500$. The flow is periodic, and on close inspection we found that the frequencies are consistent with the imaginary part of the eigenvalue at R_{-11}. Periodic flows persist until $R = R^{(1)}$, ≈ -74.0, when the period doubles; this is exemplified by figure 10, where the limit cycle for $R = -75$ is shown. Decreasing the Reynolds number further we find a second period doubling, as can be seen in figure 11, where the limit cycle for $R = -78$ is shown; this change of period takes place at $R = R^{(2)}$, ≈ -77.8. With $R = -80$ we find evidence that multiple period doubling has occurred. After some trial and error we found the next value, $R^{(3)} \approx -78.5$, of R at which the period doubles. We note that the ratio of the differences $(R^{(2)} - R^{(1)})/(R^{(3)} - R^{(2)}) \approx 5.3$. In view of the results for $R = -80$ and the closeness of 5.3 to Feigenbaum's universal constant, $\delta = 4.66920$, we anticipate an infinite sequence of period doubling which culminates in chaos at $R = R^{(\infty)}$, ≈ -78.7. (The values of $R^{(n)}$ here are unlikely to be accurate to three significant figures.) For $R = -80$ we note that there appears to be a limit cycle which is starting to show signs of a symmetric component along the line $f_{yy}(1,t,-80) + f_{yy}(-1,t,-80) = 0$ in the phase plane.

The limit cycle for $R = -85$ is shown in figure 12 and suggests the influence of *two* repellors, one corresponding to the symmetric solution I, and the other to the asymmetric solution I_{-1}. We note that the symmetric part of the orbit is becoming more pronounced. In looking at this figure and other diagrams for smaller values of R it should be remembered that for solutions I the first eigenvalue s_1 ($= q_1$) is negative but s_2 ($= r_1$) is complex with $s_3 = s_2^*$ ($= r_2$) and $\mathrm{Re}(s_2) > 0$, and also that the complex eigenfunction G_2 is an odd function. The existence of such complex eigenfunctions explains why the orbit overshoots the saddle focus I and then returns – as will be seen later, this is even more pronounced for $R < -90$. For the asymmetric solutions I_{-1} also, the first two real eigenvalues coalesce and form a complex conjugate pair of eigenvalues at $R \approx -85$; this accounts for the spiral of the orbit near the point $(-2, -11)$ corresponding to I_{-1}. On the basis of the eigenvalues shown in figure 4 it appears that I_{-1} is a saddle focus. The figure for $R = -85$ is too involved to infer the presence or absence of chaos.

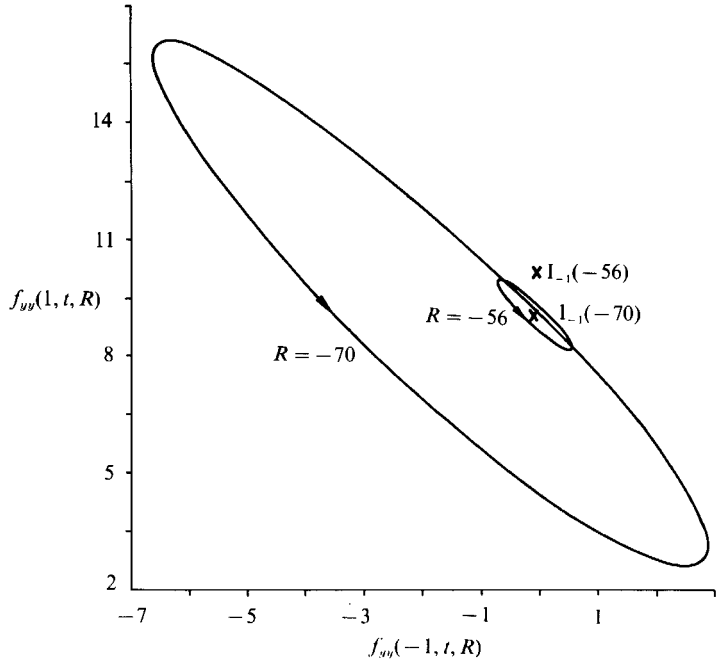

FIGURE 9. Phase planes of $f_{yy}(1,t,-56)$ and $f_{yy}(-1,t,-56)$, and of $f_{yy}(1,t,-70)$ and $f_{yy}(-1,t,-70)$ with t as parameter. In each case the flow is periodic. The unstable steady solution I_{-1} is indicated by a cross for $R=-56$ and -70.

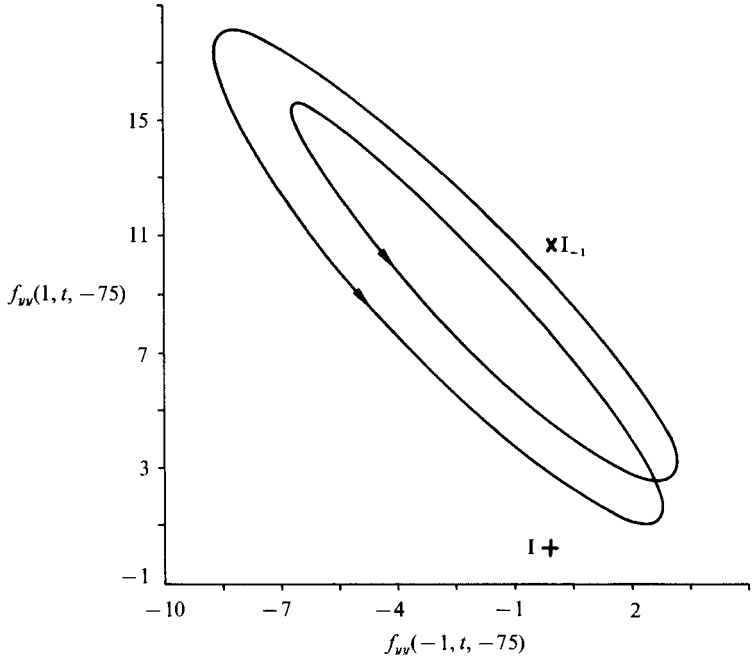

FIGURE 10. Phase plane of $f_{yy}(1,t,-75)$ and $f_{yy}(-1,t,-75)$ with t as parameter.

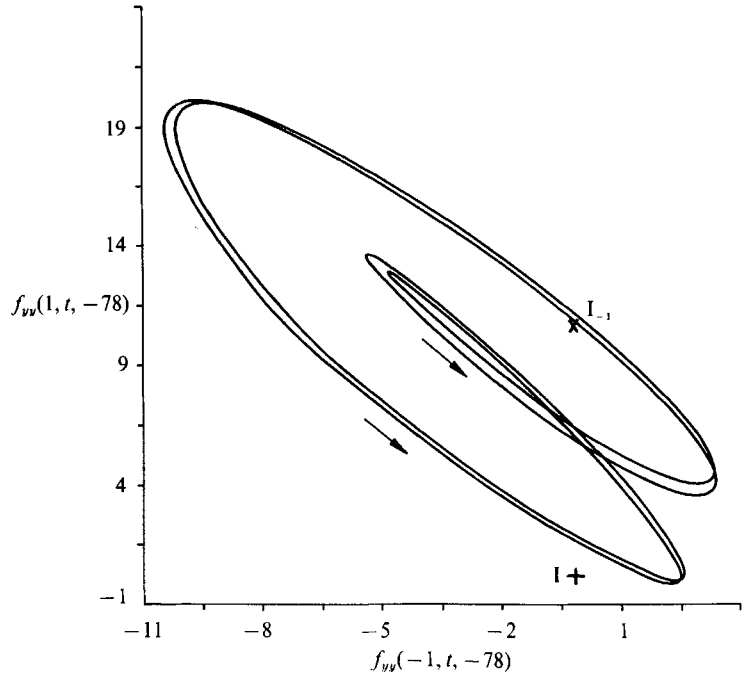

FIGURE 11. Phase plane of $f_{vv}(1,t,-78)$ and $f_{vv}(-1,t,-78)$ with t as parameter.

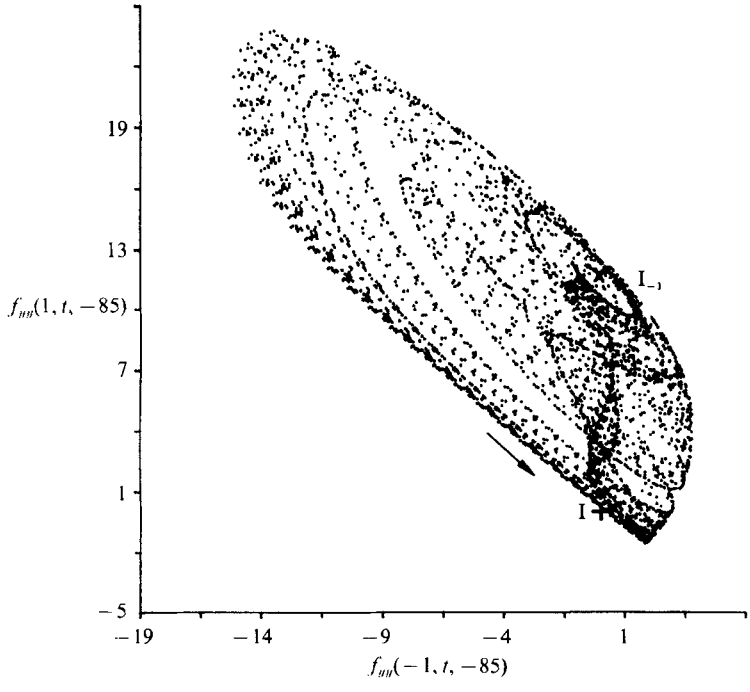

FIGURE 12. Phase plane of $f_{vv}(1,t,-85)$ and $f_{vv}(-1,t,-85)$ with t as parameter.

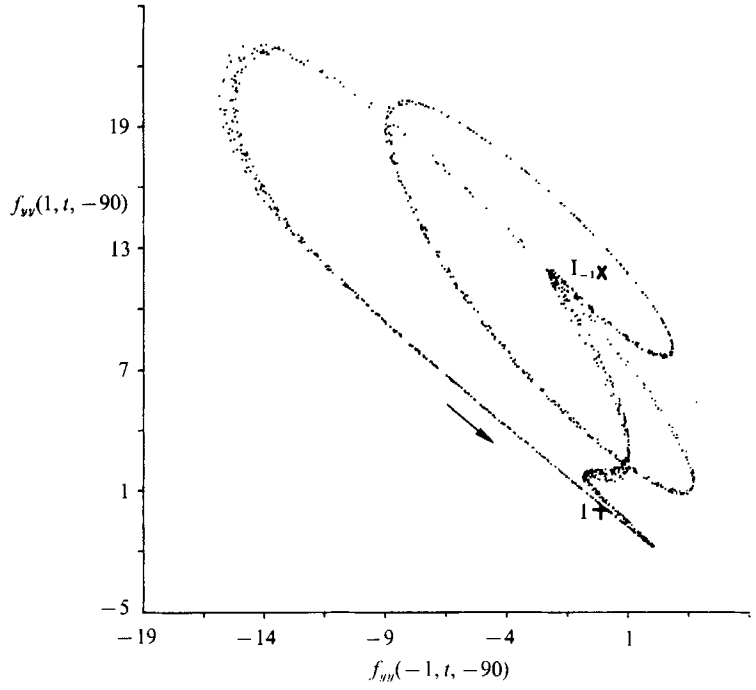

FIGURE 13. Phase plane of $f_{yy}(1, t, -90)$ and $f_{yy}(-1, t, -90)$ with t as parameter.

With $R = -90$ the plot of the phase plane shown in figure 13 looks less complicated than that for $R = -85$ but the braiding that is now clearly visible in certain regions is highly suggestive of chaos. However, our interpretation, in terms of the steady solutions I and I_{-1} and their stability characteristics, is still applicable. We note that because the real part of the unstable eigenvalue of the asymmetric steady solution is decreasing, the orbit is being repelled more vigorously near the point I_{-1}; the same arguments apply near the saddle focus I although the unstable eigenvalue of this steady solution is of course real. The plot for $R = -95$ shown in figure 14 shows a far 'cleaner' orbit with no braiding and a comparatively simple limit cycle.

We show results for $R = -100$ in figure 15. We see that the orbit of the attractor has developed some parts on the 'other side' of the symmetry line defined by $f_{yy}(-1, t, -100) + f_{yy}(1, t, -100) = 0$. Further, we note that the figure is by no means symmetric (even allowing for the different scales) and that there is the suggestion of yet more braiding. At $R < -100$ we anticipate yet more complications if only because of the origin of unstable symmetric periodic solutions at the Hopf bifurcation at $R \approx -170$ (see §3).

We complete the presentation of the numerical results of this section by displaying in figures 16 and 17 the Fourier spectra for $R = -70$, -74, -78, -78.7 and -100 corresponding to some of the critical regimes. The last figure is highly suggestive of chaos for $R = -100$.

These results seem too complex to be explained by a single simple geometrical model. It is, however, clear that the route to chaos is by period doubling, as found by Feigenbaum for one-dimensional maps and described by Glendinning (1988) for differential systems, although we have not identified any solution of period three, five

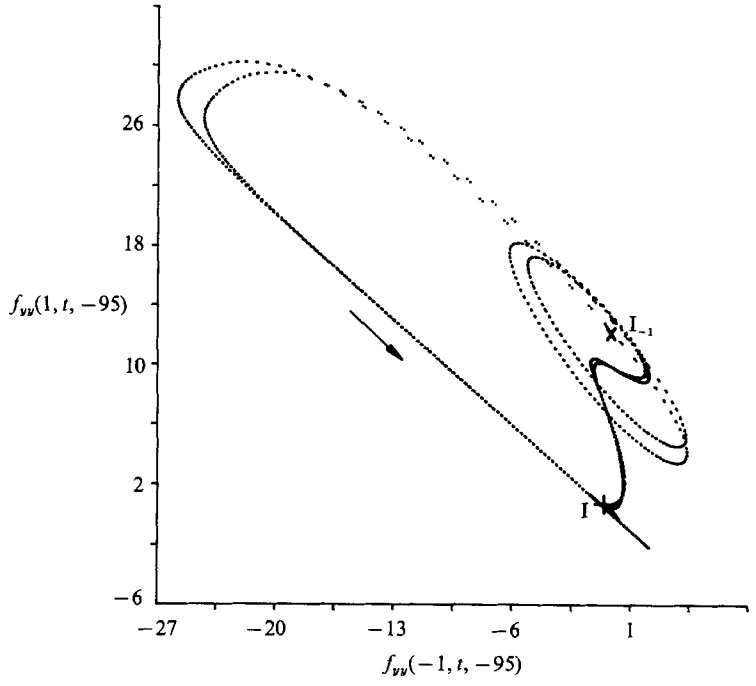

FIGURE 14. Phase plane of $f_{yy}(1, t, -95)$ and $f_{yy}(-1, t, -95)$ with t as parameter.

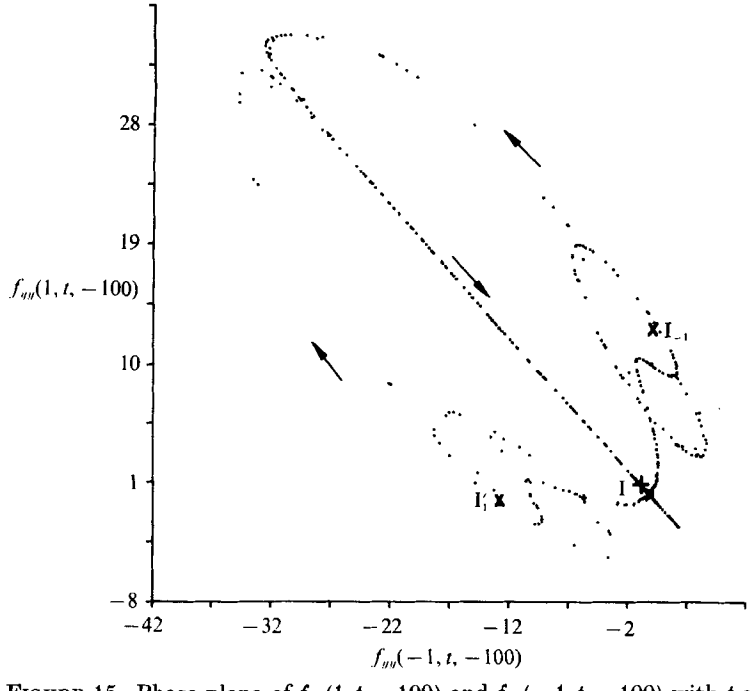

FIGURE 15. Phase plane of $f_{yy}(1, t, -100)$ and $f_{yy}(-1, t, -100)$ with t as parameter.

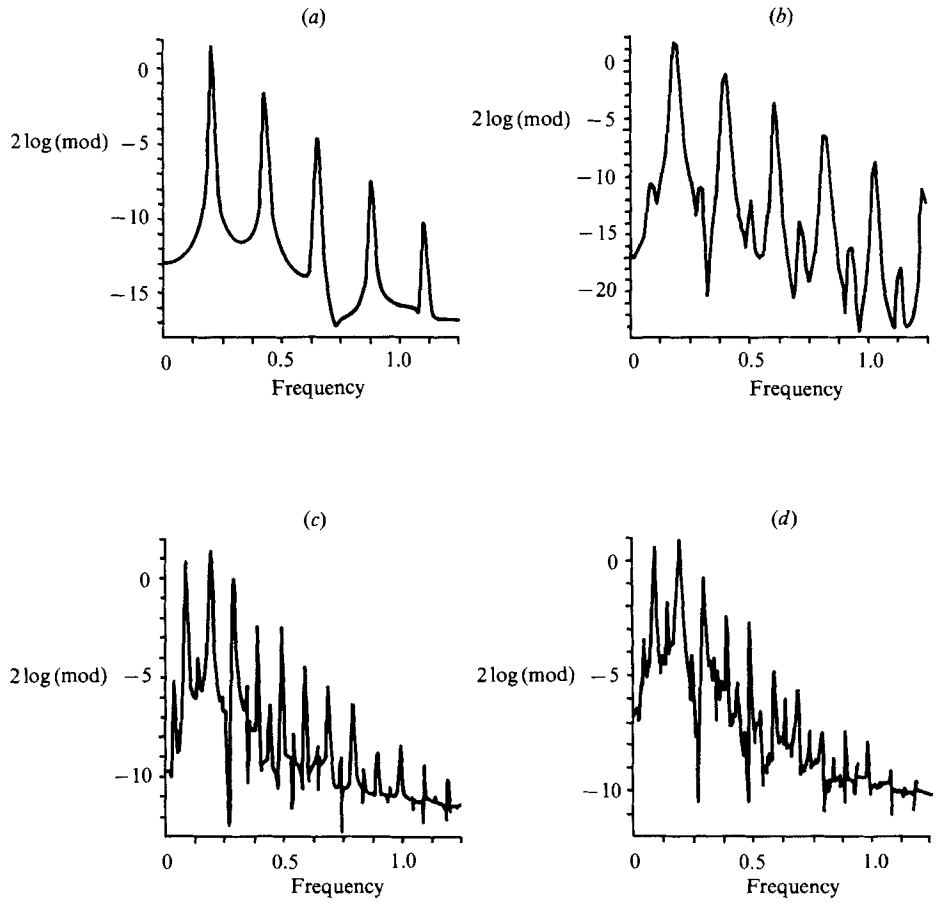

FIGURE 16. Logarithm (to base 10) of the square of the modulus of the Fourier transform of time series of $f_{yy}(1, t, R)$ versus frequency for (*a*) $R = -70$, (*b*) $R = -74$, (*c*) $R = -78$ and (*d*) $R = -78.7$.

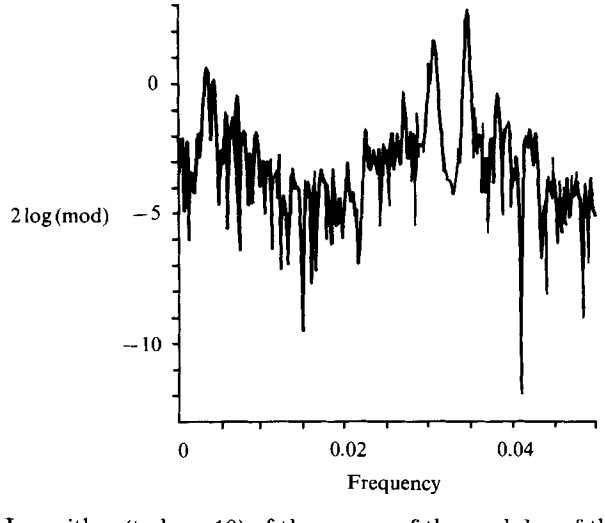

FIGURE 17. Logarithm (to base 10) of the square of the modulus of the Fourier transform of time series of $f_{yy}(1, t, -100)$ versus frequency.

etc. for $R < R^{(\infty)}$. Indeed, many details, e.g. the 'windows' of periodic and chaotic solutions for $-100 < R < -79$, remain to be carefully elucidated.

Note that the orbits go close to both the fixed points I and I_{-1} for $-100 < R < -90$, so we now need a pair of equations, analogous to (7.1), to model the attractor piecewise in this regime. To this end we write

$$f(y, t, R) = F^{(\mathrm{I})}(y, R) + \sum_{n=1}^{4} T_n^{(\mathrm{I})}(t)\, G_n^{(\mathrm{I})}(y, R) \tag{7.2}$$

and

$$f(y, t, R) = F^{(\mathrm{I}_{-1})}(y, R) + \sum_{n=1}^{4} T_n^{(\mathrm{I}_{-1})}(t)\, G_n^{(\mathrm{I}_{-1})}(y, R), \tag{7.3}$$

where $G_n^{(N)}(y, R)$ is the nth eigenfunction for the flow of type N with solution $F^{(N)}(y, R)$, and $T_n^{(N)}(t)$ will behave like $\exp(s_n^{(N)} t)$ when the solution is close to that of type N. We note that $G_2^{(\mathrm{I})}$ and $G_3^{(\mathrm{I})}$ together with their associated eigenvalues are complex (see figure 2) and this is mirrored in the phase plots for $R = -90$, -95, and -100 near the saddle focus I. Similarly, since $G_1^{(\mathrm{I}_{-1})}$, $G_2^{(\mathrm{I}_{-1})}$ and their associated eigenvalues are complex and, further, are unstable (see figure 4), we see spirals around I_{-1}.

8. Conclusions

The foregoing sections describe a rich variety of bifurcations for a class of exact solutions of the Navier–Stokes equations. In particular, for $\chi = 1$, the onset of chaos when two homoclinic orbits break up as R increases and the Feigenbaum route to chaos as R decreases are described in §7. The routes in which there is a sequence of bifurcations from symmetric steady, to asymmetric steady, to periodic, to chaotic, to other periodic, to chaotic solutions etc. are new in detail and as being among a class of exact solutions of the Navier–Stokes equations. We contrast this behaviour to that encountered when $\chi = 0$ corresponding to the porous channel (see ZDB) in which only the first route exists – for $R < 0$ the symmetric flow is found to be stable to perturbations of the form (1.14).

The above are accordingly possible routes to chaos of real flows. However, various practical points must be borne in mind. First, although accelerating walls have a long history in the theory of viscous flow, it is not feasible to design a channel with two accelerating walls; the construction of even a single accelerating wall presents considerable difficulty (see §1) so the only likely laboratory realization is for the special case ($\chi = 0$) of fixed channel walls. Even then an experiment would necessarily be in a channel of finite span and length, so that the assumed similarity solutions would at best be only approximations to real flows along a wide long channel. However, the results of §6 show that at least some three-dimensional disturbances are more stable than two-dimensional ones. Further, because it occurs at such low values of the Reynolds number, so that for a channel of moderate length the fluid velocities are small enough to be realizable, the route to chaos may be observable and thereby offer a rare insight into transition to turbulence.

This paper has been chiefly concerned with the case of symmetric boundary conditions, which is governed by the two dimensionless parameters, χ and R. However, we have briefly considered asymmetric boundary conditions (4.19), and it should be recognized that with different values of uniform suction at, and acceleration of, each wall of the channel the similarity solutions are governed by four independent dimensionless parameters. Two special cases are currently being investigated: (i)

S. M. Cox is examining the case when the walls of the channel are fixed but with unequal suction there; and (ii) P. Watson is examining the case when the flow is driven by impermeable walls accelerating asymmetrically. Consideration of the general case must await a future occasion.

We are grateful to Dr Martin Berzins for making available to us the algorithms to solve the nonlinear diffusion equation of §7, and E.B.B.W. to the SERC for the award of an Advanced Course Studentship.

Appendix

For the special case $V+Eh=0$, equivalent to infinite χ, we may write $F=-\chi\bar{F}$ and $R=-\chi^{-1}\bar{R}$ so that the system (1.8), (1.9) becomes

$$\bar{F}^{\mathrm{iv}}+\bar{R}(\bar{F}\bar{F}'''-\bar{F}'\bar{F}'')=0, \tag{A 1}$$

$$\mathbf{B}\bar{F}=[(1-\chi^{-1}),\ -1,\ -(1-\chi^{-1}),-1]^{\mathrm{T}}. \tag{A 2}$$

In the limit as $\chi\to-\infty$ this system has the simple solution $\bar{F}(y,\bar{R})=-y$, for all $\bar{R}$, a solution which clearly represents a symmetric flow of type I.

Substituting this analytic result into the eigenvalue equation (1.15) leads to the general solution

$$G=b_1\,y+b_2+\exp\,(\tfrac{1}{4}\bar{R}y^2)\{b_3\,U(\bar{s}-\tfrac{7}{2},\bar{R}^{\frac{1}{2}}y)+b_4\,V(\bar{s}-\tfrac{7}{2},\bar{R}^{\frac{1}{2}}y)\}, \tag{A 3}$$

where U, V are the parabolic cylinder functions and $\bar{s}=-\chi^{-1}s$. (In fact the Hermite polynomial $G=H_{3-\bar{s}}\{(\frac{1}{2}\bar{R})^{\frac{1}{2}}y\}$ satisfies (1.15) when $3-\bar{s}$ is a non-positive integer, and the third and fourth solutions of (A 3) give this polynomial for integral $\bar{s}\leqslant 1$.) We note in particular that $\bar{s}=0$, $b_1=b_3=0$ corresponds to the antisymmetric mode at marginal stability when $\bar{R}=\bar{R}_1$, and that application of the condition $G'(1,\bar{R}_1)=0$ and use of the recurrence relations for the function V gives $V(-\frac{5}{2},\bar{R}_1^{\frac{1}{2}})=0$. This condition identifies the value of $\bar{R}$ at the pitchfork bifurcation: from tables (Abramowitz & Stegun 1964) we find $\bar{R}_1^{\frac{1}{2}}\approx 2.124$. Thus $R_1\sim-4.511\chi^{-1}$ as $\chi\to-\infty$. Direct numerical solution of the eigenvalue problem with $F(y,\bar{R})=-y$ gave the result $\bar{R}_1=4.5118$ when $\bar{s}=0$, i.e. $R_1\sim-4.5118\chi^{-1}$ as $\chi\to-\infty$.

When boundary conditions (A 2) are applied to the general solution (A 3) the eigenvalues $\bar{s}(\bar{R})$ may be determined in principle, but in practice it is easier to identify the values of $\bar{R}$ corresponding to integer values of $\bar{s}$.

We note that $F(y,R)=-y$ is also an exact solution of (A 1) subject to asymmetric boundary conditions including, for example, $F(\mu)=-\mu$, $F'(\mu)=F(1)=F'(1)=-1$. Substituting this exact solution into the eigenvalue problem (1.15), (1.16) and using the methods of §2.1, we have found the behaviour of the eigenvalues for small R. For general values of R, (1.15) has a solution of the form (A 3) but we have not found an analytic solution of the whole eigenvalue problem. Moreover, the analysis suggests that there are no real eigenvalues as $R\to\infty$. Also it appears that the pitchfork bifurcation for $\mu=-1$ is unfolded into transcritical bifurcations for small $1+\mu>0$.

REFERENCES

Abramowitz, M. & Stegun, I. A. 1964 *Handbook of Mathematical Functions*. Washington: National Bureau of Standards.

Banks, W. H. H., Drazin, P. G. & Zaturska, M. B. 1988 On perturbations of Jeffery–Hamel flow. *J. Fluid Mech.* **186**, 559–581.

BERMAN, A. S. 1953 Laminar flow in channels with porous walls. *J. Appl. Phys.* **24**, 1232–1235.

BERZINS, M. & DEW, P. M. 1989 Chebyshev polynomial software for elliptic-parabolic systems of P.D.E.S. *A.C.M. Trans. Math. Software* (in the press).

BRADY, J. F. 1981 Inertial effects in closed cavity flows and their influence on drop breakup. Ph.D. thesis, Stanford University.

BRADY, J. F. & ACRIVOS, A. 1981 Steady flow in a channel or tube with an accelerating surface velocity. An exact solution to the Navier–Stokes equations with reverse flow. *J. Fluid Mech.* **112**, 127–150.

DURLOFSKY, L. & BRADY, J. F. 1984 The spatial stability of a class of similarity solutions. *Phys. Fluids* **27**, 1068–1076.

GLENDINNING, P. 1988 Global bifurcations in flows. In *New Directions in Dynamical Systems* (ed. T. Bedford & J. Swift), pp. 120–149. Cambridge University Press.

STUART, J. T. 1988 Nonlinear Euler partial differential equations: singularities in their solution. In *A Symposium to Honor C. C. Lin* (ed. D. J. Benney, F. H. Shu & C. Yuan), pp. 81–95. Singapore: World Scientific Publishing.

TERRILL, R. M. 1964 Laminar flow in a uniformly porous channel. *Aeronaut. Q.* **15**, 299–310.

TERRILL, R. M. 1965 Laminar flow in a uniformly porous channel with large injection. *Aeronaut. Q.* **16**, 323–332.

WATSON, E. B. B. 1987 Laminar flow in a channel with accelerating walls. M.Sc. thesis, University of Bristol.

ZATURSKA, M. B., DRAZIN, P. G. & BANKS, W. H. H. 1988 On the flow of a viscous fluid driven along a channel by suction at porous walls. *Fluid Dyn. Res.* **4**, 151–178 (referred to as ZDB).